The Atlantic Meridional Overturning Circulation in High-Resolution Models

Joël J. -M Hirschi, Bernard Barnier, Claus Böning, Arne Biastoch, Adam T Blaker, Andrew Coward, Sergey Danilov, Sybren Drijfhout, Klaus Getzlaff, Stephen M Griffies, et al.

JGR Oceans

REVIEW ARTICLE
10.1029/2019JC015522

Special Section:
Atlantic Meridional Overturning Circulation: Reviews of Observational and Modeling Advances

The Atlantic Meridional Overturning Circulation in High-Resolution Models

Joël J.-M. Hirschi[1], Bernard Barnier[2], Claus Böning[3], Arne Biastoch[3], Adam T. Blaker[1], Andrew Coward[1], Sergey Danilov[4], Sybren Drijfhout[5], Klaus Getzlaff[3], Stephen M. Griffies[6], Hiroyasu Hasumi[7], Helene Hewitt[8], Doroteaciro Iovino[9], Takao Kawasaki[7], Andrew E. Kiss[10], Nikolay Koldunov[4], Alice Marzocchi[1], Jennifer V. Mecking[1], Ben Moat[1], Jean-Marc Molines[2], Paul G. Myers[11], Thierry Penduff[2], Malcolm Roberts[8], Anne-Marie Treguier[12], Dmitry V. Sein[4], Dmitry Sidorenko[4], Justin Small[13], Paul Spence[14], LuAnne Thompson[15], Wilbert Weijer[16], and Xiaobiao Xu[17]

[1]National Oceanography Centre, Southampton, UK, [2]Université Grenoble Alpes, CNRS, IRD, Grenoble-INP, IGE, Grenoble, France, [3]Geomar, Kiel, Germany, [4]Alfred Wegener Institute for Polar and Marine Research, Bremerhaven, Germany, [5]University of Southampton, Ocean and Earth Science, Southampton, UK, [6]Atmosphere & Ocean Sciences Program, NOAA/GFDL + Princeton University, Princeton, NJ, USA, [7]Atmosphere and Ocean Research Institute, The University of Tokyo, Tokyo, Japan, [8]Met Office, Exeter, UK, [9]Ocean Modeling and Data Assimilation Division, Centro Euro-Mediterraneo sui Cambiamenti Climatici, Italy, [10]Research School of Earth Sciences, Australian National University + ARC Centre of Excellence for Climate Extremes, Canberra, ACT, Australia, [11]Department of Earth and Atmospheric Sciences, University of Alberta, Edmonton, Alberta, Canada, [12]Laboratoire d'océanographie Physique et Spatiale, CNRS, Brest, France, [13]NCAR/UCAR, Boulder, CO, USA, [14]Climate Change Research Centre, University of New South Wales + ARC Centre of Excellence for Climate Extremes, Sydney, New South Wales, Australia, [15]University of Washington, School of Oceanography, Seattle, WA, USA, [16]Los Alamos National Laboratory, Los Alamos, NM, USA, [17]Florida State University, Center for Ocean-Atmospheric Predictions Studies, Tallahassee, FL, USA

Key Points:
- Observations and high-resolution models have changed view on the AMOC pathways
- High-resolution models suggest the presence of previously unknown high-frequency AMOC variability
- High-resolution models allow to estimate the intrinsic/chaotic component of the AMOC

Correspondence to:
J. J.-M. Hirschi,
joel.hirschi@noc.ac.uk

Citation:
Hirschi, J. J.-M., Barnier, B., Böning, C., Biastoch, A., Blaker, A. T., Coward, A., et al. (2020). The Atlantic meridional overturning circulation in high-resolution models. *Journal of Geophysical Research: Oceans*, *125*, e2019JC015522. https://doi.org/10.1029/2019JC015522

Received 24 JUL 2019
Accepted 20 JAN 2020
Accepted article online 27 JAN 2020

Abstract The Atlantic meridional overturning circulation (AMOC) represents the zonally integrated stream function of meridional volume transport in the Atlantic Basin. The AMOC plays an important role in transporting heat meridionally in the climate system. Observations suggest a heat transport by the AMOC of 1.3 PW at 26°N—a latitude which is close to where the Atlantic northward heat transport is thought to reach its maximum. This shapes the climate of the North Atlantic region as we know it today. In recent years there has been significant progress both in our ability to observe the AMOC in nature and to simulate it in numerical models. Most previous modeling investigations of the AMOC and its impact on climate have relied on models with horizontal resolution that does not resolve ocean mesoscale eddies and the dynamics of the Gulf Stream/North Atlantic Current system. As a result of recent increases in computing power, models are now being run that are able to represent mesoscale ocean dynamics and the circulation features that rely on them. The aim of this review is to describe new insights into the AMOC provided by high-resolution models. Furthermore, we will describe how high-resolution model simulations can help resolve outstanding challenges in our understanding of the AMOC.

1. Introduction

The Atlantic Meridional Overturning Circulation (AMOC) is often defined as the zonally integrated and vertically accumulated meridional ocean volume transport in the Atlantic Ocean. The main reason why the AMOC has been the subject of many studies is because of its role in the climate system (e.g., Jackson et al., 2015; Stocker, 2013). The AMOC is a major contributor to the redistribution of heat from the low latitudes where there is a net heat gain owing to strong solar radiation to the higher latitudes where there is a net heat loss to the atmosphere. In the North Atlantic the AMOC transports about 0.5 PW across the equator, increasing to a maximum of 1.3 PW of heat northward at 26°N (Hall & Bryden, 1980; Johns et al., 2011; McCarthy et al., 2015; Baringer et al., 2018). As a result, the AMOC is thought to moderate the climate of western and northern Europe with effects felt well into Eurasia (e.g., Rahmstorf & Ganopolski, 1999).

The paleoclimate record suggests that the AMOC is likely to have undergone major rearrangements in its structure between glacial and interglacial periods and has been subject to abrupt (i.e., multidecadal/centennial to millennial timescales) changes, as reviewed by Lynch-Stieglitz (2017) and Moffa-Sánchez et al. (2019). For instance, during the last glacial period from 115,000 to 11,700 years ago, Greenland Ice-core records show repeated pronounced warming and cooling events (e.g., Dansgaard–Oeschger and Heinrich events; Heinrich, 1988; Dansgaard et al., 1993) that are superposed on the longer climate cycles from glacial cycles. Whereas the factors that caused these events are still unclear, analyses of multiple proxies have suggested a connection to the AMOC (e.g., Bond et al., 1999; Gebbie, 2014; Amrhein et al., 2018). A particularly interesting and important point raised in these studies is whether abrupt AMOC changes seen in the past may happen in the present or future climate.

The paleo record suggests that the AMOC may be subject to rapid change in strength and stability with consequent changes in AMOC-related meridional heat transport (e.g., Jansen et al., 2018; Thornalley et al., 2018). Currently, climate projections suggest that the AMOC will weaken (but not collapse) in response to global warming (Drijfhout et al., 2012; Reintges et al., 2017; Stocker et al., 2014). However, whether the current generation of low-resolution climate models adequately simulates the sensitivity of the AMOC to a warming climate is still a matter of debate (e.g., Caesar et al., 2018; Rahmstorf et al., 2015) with some authors suggesting that the sensitivity in nature could be higher than previously thought (Heuzé, 2017; Reintges et al., 2017). For more exhaustive overviews about the AMOC and mechanisms driving its strength and variability we refer the reader to comprehensive reviews such as Lumpkin and Speer (2007), Kuhlbrodt et al. (2007), Buckley and Marshall (2016), Zhang et al. (2019), Johnson et al. (2019) and Weijer et al. (2019).

The observational quantification of the components of AMOC has included multiple efforts at different locations within the Atlantic basin. Since the Meteor expedition in the 1920s, we have known that one can infer geostrophic transports across a section from the end points (e.g., Merz, 1925). Moored instruments at key locations at the basin margins are sufficient to estimate strength, vertical structure, and variability of geostrophic transports between the end points of a mooring array line (e.g., Hirschi et al., 2003; Lee & Marotzke, 1998; Rayner et al., 2011). In the OVIDE program that began in 1997 hydrographic sections are used to quantify the transports between Greenland and Portugal (Mercier et al., 2015). The MOVE array began deploying moorings in 2000 that allow an estimate of the deep southward transport of AMOC at 14°N (Elipot et al., 2014; Kanzow et al., 2006).

Repeat hydrographic sections (observations of temperature, salinity, and depth) along with cabled measurement of the transport of the Florida Current in Florida Straits (e.g., Bryden et al., 2005) can give estimates of AMOC near 26°N. However, the infrequent hydrographic sections make it likely that AMOC variability inferred from such sections is aliased in time. Since 2004 a continuous observing system for the AMOC has been deployed in the North Atlantic across 26.5°N (Cunningham et al., 2007; Kanzow et al., 2007; McCarthy et al., 2012, 2015). This system provides estimates of the strength, variability, and vertical structure of the AMOC (Smeed et al., 2014, 2018) and provided the first observational evidence that the AMOC can undergo substantial variations on short (i.e., subannual to interannual) timescales (Cunningham et al., 2007; Kanzow et al., 2007, 2010; McCarthy et al., 2012; Smeed et al., 2014, 2018; Bryden et al., 2014).

In the framework of the SAMOC (South Atlantic Meridional Overturning Circulation) program, a combination of different sections, moorings, and satellite altimetry is used to provide estimates of strength and variability of the AMOC in the South Atlantic (e.g., Dong et al., 2009; Perez et al., 2011, 2015; Pérez et al., 2013). Using a variety of platforms, AMOC measurements at other latitudes and locations have been implemented in the last decade. OSNAP (Overturning in the Subpolar North Atlantic) provides a framework for estimating the AMOC in the subpolar North Atlantic since 2014 (Holliday et al., 2018; Lozier et al., 2017; Lozier et al., 2019).

At some latitudes AMOC time series have been extended through the combination of in situ measurements listed above along with Argo measurements and satellite altimetry that in some cases allows extending the measurements back to the beginning of the altimeter record in 1993 (e.g., Willis 2010, Frajka-Williams, 2015, Mercier et al., 2015, and Perez et al., 2018). These measurements provide invaluable information about the AMOC and are unique benchmarks against which models can be evaluated (e.g., Blaker et al., 2015; Duchez et al., 2014; Xu et al., 2014) at the corresponding locations. While this wealth of observations opens up the prospect of being able to understand how the ocean circulation and

the AMOC in particular impact Atlantic-wide changes in properties such as heat, freshwater, and carbon (Frajka-Williams et al., 2019; Perez et al., 2018), the current observational network is not sufficient to study the full four-dimensional spatiotemporal velocity structure that makes up the AMOC structure. How and on what timescales AMOC variability at different latitudes is related cannot yet be conclusively assessed from observational records.

Ocean models, ranging from simple box models to complex general circulation models, have informed our understanding of the mechanisms that drive the AMOC and its variability (e.g., Bingham et al., 2007; Böning et al., 2006; Robson et al., 2014). Box models with analytical or numerical solutions (e.g., Stommel, 1961; Marotzke et al., 1988; Griffies & Tziperman, 1995; Longworth et al., 2005; Wood et al., 2019; Alkhayuon et al., 2019) were and still are useful (and popular) tools to illustrate and study possible AMOC behavior. Within their limitations (spatial resolution, physical assumptions, parameterisation choice, etc.) general circulation models provide self-consistent four-dimensional data sets for the ocean circulation (including the AMOC); they allow us to "play" with different scenarios, test likely sensitivities in the climate system, in some instances they can guide observational efforts (e.g., Hirschi et al., 2003), and can point to currents and circulation features before these are observed in nature (e.g., Aksenov et al., 2011; Treguier et al., 2005). However, models inevitably have shortcomings in their ability to represent the physics of nature. In coarse-resolution models (order 1° or coarser) currents, which are known to be jet like in the real ocean, are simulated as broad and diffuse currents with velocities much weaker than observed and they are often in the wrong location and have the wrong vertical structure. In addition, mesoscale ocean eddies as detected by satellite altimetry (Chelton et al., 2007) are not resolved. Nearly all the models included in the CMIP5 climate projections use coarse ocean model resolution.

In parallel to the increase in the availability of high-quality AMOC estimates, there has been a massive increase in high-performance computing (HPC) resources and in our ability to exploit them to simulate the natural world. The latest generation of ocean and coupled ocean-atmosphere models is being run at resolutions sufficient to simulate the ocean circulation with a remarkable level of detail (e.g., Böning et al., 2016; Haarsma et al., 2016; Iovino et al., 2016; Marzocchi et al., 2015; Moat et al., 2016; Rieck et al., 2019; Sein et al., 2016, 2017). Features such as ocean mesoscale eddies are now increasingly present in ocean and ocean-atmosphere simulations. In some instances increased resolution results in better representation of boundary currents such as the Gulf Stream, the Agulhas-, Brazil-, and Malvinas currents (e.g., Biastoch et al., 2018; Griffies et al., 2015; Hewitt et al., 2016; Murakami et al., 2015; Sein et al., 2018; Small et al., 2014). Similarly, fronts, and the associated gradients of temperature and salinity, are more sharply defined. Improved representation of oceanic surface temperature gradients is of particular interest in coupled simulations, where the ability to simulate a more realistic imprint of the ocean onto the atmosphere is a potential source of improvement in forecasting systems. Satellite observations and reanalyses have shown that the ocean front associated with the Gulf Stream affects the atmosphere all the way up to the tropopause (Minobe et al., 2008; Minobe et al., 2010; Siqueira & Kirtman, 2016). In model simulations a similar effect is only found when the underlying ocean represents the sharp temperature front across the Gulf Stream (Kuwano-Yoshida et al., 2010; Minobe et al., 2008). In addition, the presence of mesoscale eddies changes the character of the simulated variability across timescales (Penduff et al., 2010). The latest generation of coupled ocean-atmosphere models now increasingly uses an ocean component that is "eddy permitting" (nominal 0.25° resolution) or in some instances "eddy rich" (Roberts et al., 2018, nominal 0.1° resolution).

A noteworthy benefit that emerged from the use of a higher-resolution model is found in seasonal forecasting where for the first time a significant skill is found for winter forecasts for the North Atlantic Oscillation (Dunstone et al., 2016; Scaife et al., 2014). However, the physical mechanisms for this breakthrough in seasonal forecasting are not yet clear. A major change in the model used to produce the forecasts was the use of an eddy-permitting ocean model. The resulting improvement in the position of ocean currents and fronts in the North Atlantic is thought to play a key role. However, the representation of the dense overflow across the sill separating the European Nordic Seas from the subpolar North Atlantic remains a challenge owing to the small-scale processes that control the interaction of small-scale topography and entrainment into the overflow plume (Legg et al., 2009).

The goal of this review is to evaluate how ocean simulations in the eddying regime inform our understanding of the mean, structure, and variability of the AMOC. We emphasize that each level of complexity from very

simple, highly idealized (analytical and numerical) models to the latest state-of-the-art high-resolution numerical models that run on massively parallel HPC architectures can provide valuable insights in our quest to better understand the role of the AMOC in the global climate system. This review is structured as follows: Section 2 shows results from a set of high-resolution models to illustrate how the AMOC is represented in this latest generation of models. Section 3 focuses on the insight gained from studying AMOC in high-resolution models. Section 4 summarizes areas in need of improvement. Finally, section 5 outlines areas where high-resolution simulations can inform future research. Finally, a brief conclusion is given in section 6.

2. AMOC in High-Resolution Models: Where Do We Stand?

More than three decades have passed since the pioneering regional and global eddying ocean simulations were performed (Semtner & Chervin, 1988; Semtner & Mintz, 1977). Owing to computational cost, these early eddying simulations were run for short periods. The integration length was sufficient to develop the mesoscale eddy field and sharp boundary currents but too short for studies of quantities, such as the AMOC, that require that the deep ocean circulation is allowed to adjust. Furthermore, to keep computational cost manageable, these simulations used a relatively small number of vertical levels, and the main focus was on the surface circulation. These first efforts at high-resolution ocean modeling were followed by programs such as the Fine Resolution Antarctic Model (The FRAM GROUP, 1991; Stevens, 1991; Killworth, 1992; Lutjeharms et al., 1995), the Ocean Circulation and Climate Advanced Modelling Project (Saunders et al., 1999; Webb et al., 1997; Webb et al., 1998), the Family of Linked Atlantic Model Experiments (Dengg et al., 1999), the Parallel Ocean Program (Maltrud et al., 1998; Smith et al., 2000), the CLIPPER Project (Treguier et al., 1999), and the Miami Isopycnic Coordinate Ocean Model (Paiva et al., 1999). Both integration length and vertical resolution were increased in these modeling efforts, allowing studies of eddy statistics, circulation structure, and variability in the Southern Ocean (e.g., Stevens, 1991; Killworth, 1992; Lutjeharms & Webb, 1995), the North Atlantic (e.g., Böning & Herrmann, 1994; Eden & Willebrand, 2001; McCLean et al., 2002; Böning et al., 2003; Treguier et al., 2005), or the Pacific (e.g., Richards et al., 2006). During the last decade or so, there has been a consolidation of the modeling efforts mentioned above with longer simulations (multidecadal and sometimes even longer) that are eddy rich and even ensembles performed at eddy-permitting or eddy-rich resolutions (e.g., Bessières et al., 2017; Iovino et al., 2016; Marzocchi et al., 2015). These simulations also use a higher number of vertical levels/layers. Whereas early high-resolution ocean models were all run in ocean-only mode, significant efforts have been and are being dedicated to coupling eddy-permitting and increasingly eddy-rich ocean components to an atmosphere model (e.g., Delworth et al., 2012; Griffies et al., 2015; Haarsma et al., 2016; Hewitt et al., 2016; Ito et al., 2015; Roberts et al., 2019; Winton et al., 2014). This coupling allows the community not only to address questions around the ocean circulation and its variability but also to refine our understanding of how, where, and on what timescales the ocean interacts with the atmospheric circulation and vice versa.

In this review, we use output from a large (but not exhaustive) set of state-of-the-art high-resolution ocean-only and coupled ocean-atmosphere simulations to examine how these models represent the AMOC and its variability (Table 1). Multimodel intercomparisons of the AMOC have been done before (e.g., Danabasoglu et al., 2014) but not for high resolution (i.e., eddying models). The goal here is not to provide an in-depth multimodel intercomparison but to use output from current high-resolution models to provide an overview of the range of solutions obtained for the AMOC.

The AMOC (ψ) is calculated from the model velocity fields as follows:

$$\psi_{(y,\zeta)} = \int_{x_w}^{xe} \mathrm{d}x \int_{z(x,y,\zeta)}^{\eta} \mathrm{d}z' v(x,y,z'),$$

where v is the meridional velocity component; x_e, $x_w$are the eastern and western limits of the zonal integration; and η is the free surface height. The lower limit, $z(x,y,\zeta)$, can denote a geopotential level ($\zeta = z$) or the depth of any sea water property such as sea water density referenced to a given pressure (e.g., $\zeta = \sigma_2$) (Hirst et al., 1996; Nurser & Lee, 2004; Zika et al., 2012; Danabasoglu et al., 2014). As the focus of this review is the AMOC this integration is limited to the meridionally bounded portion of the Atlantic Basin (including the Mediterranean and Baltic Seas) with the southernmost point of the Cape of Good Hope. In the remainder of this review we will refer to the AMOC in depth and density coordinates as $\psi(z)$ and $\psi(\sigma_2)$, respectively.

Table 1
Overview of the High-Resolution Simulations Used to Illustrate Aspects of the AMOC in this Review

Model (institute)	Grid spacing (deg) and grid		Ocean only	Coupled	Regional	Global	Integrations	Reference (s)
	Horiz.	Vert.						
FESOM (AWI)	Unstructured 0.25–1	48	X			X	1948–2007 (COREII)	Danilov et al. (2004) Sein et al. (2016, 2017, 2018)
	Unstructured 0.1–0.6	48	X			X	1948–2007 (COREII)	
	Unstructured 0.25–1	48		T63		X	1950–2099	
	Unstructured 0.1–0.6	48		T63		X	1950–2099	
CESM-H (NCAR)	0.1	62		CAM5 0.25		X	100 years (year 2000 forcing)	Small et al. (2014, 2018)
ACCESS-OM2-1	1	50 (z*)	X			X	300 years (five repeats of JRA55-do 1958–2017)	Kiss et al. (2020)
ACCESS-OM2-025	0.25	50 (z*)	X			X	300 years (five repeats of JRA55-do 1958–2017)	
ACCESS-OM2-01	0.1	50 (z*)	X			X	33 years (JRA55-do 1985–2017)	
HYCOM	0.08	hybrid iso/sig/z	X			X		Xu et al. (2012, 2013, 2014)
NEMO-ORCA (MEOM Team, Uni Grenoble)	0.25	46	X			X	327 years (normal year)	Grégorio et al. (2015) Bessières et al. (2017)
	0.25	75	X			X	50 × 1958–2015 (DFS5.2)	Leroux et al. (2018)
	0.25	75	X			X	330 years (normal year)	
	0.083	75	X			X	1958–2007 (DFS4.4)	
NEMO-VIKING20X (GEOMAR)	0.05	46	X		X (nested Atl.)	X (global 0.25)	1958–2009 (COREII)	Böning et al. (2016) Rieck et al. (2019)
	0.05	46	X		X (nested Atl.)	X (global 0.25)	1980–2018 (JRA55-do)	
	0.25	46	X			X (global 0.25)	1958–2016 (JRA55-do)	
NEMO ANNA0083 (Uni Alberta)	0.083	50	X		X (20S to Bering Strait)	X	2002–2018	Müller et al. (2017) Courtois et al. (2017) Hu et al. (2018)
NEMO-ORCA (NOC-UK Met Office)	0.083	75	X			X	1958–2015 (DFS5.2)	Marzocchi et al., 2015
	0.25	75		N216		X	300 years	Hewitt et al. (2016)
	0.083	75		N512		X	1950–2050 (year 1950 forcing)	Moat et al. (2016) Roberts et al. (2019)
MIROC (AORI-Uni Tokyo)	0.25	63		T85		X	>6,000 years (normal year)	Tatebe et al. (2019)
COCO	1		X				1958–2015 (JRA55-do)	
	1		X				>500 years (normal year)	
	0.25		X				>100 years (normal year)	
	0.17		X				1958–1979 (cont.) (JRA55-do)	
	0.17		X				>100 years (PI run)	

Note. Note that some low-resolution versions are also included as these allow us to better assess improvements/changes seen at high resolution. Ocean-only simulations are forced with the reanalysis products CORE II (e.g., Griffies et al., 2009), DFS (Brodeau et al., 2010), and JRA55-do (Tsujino et al., 2018).

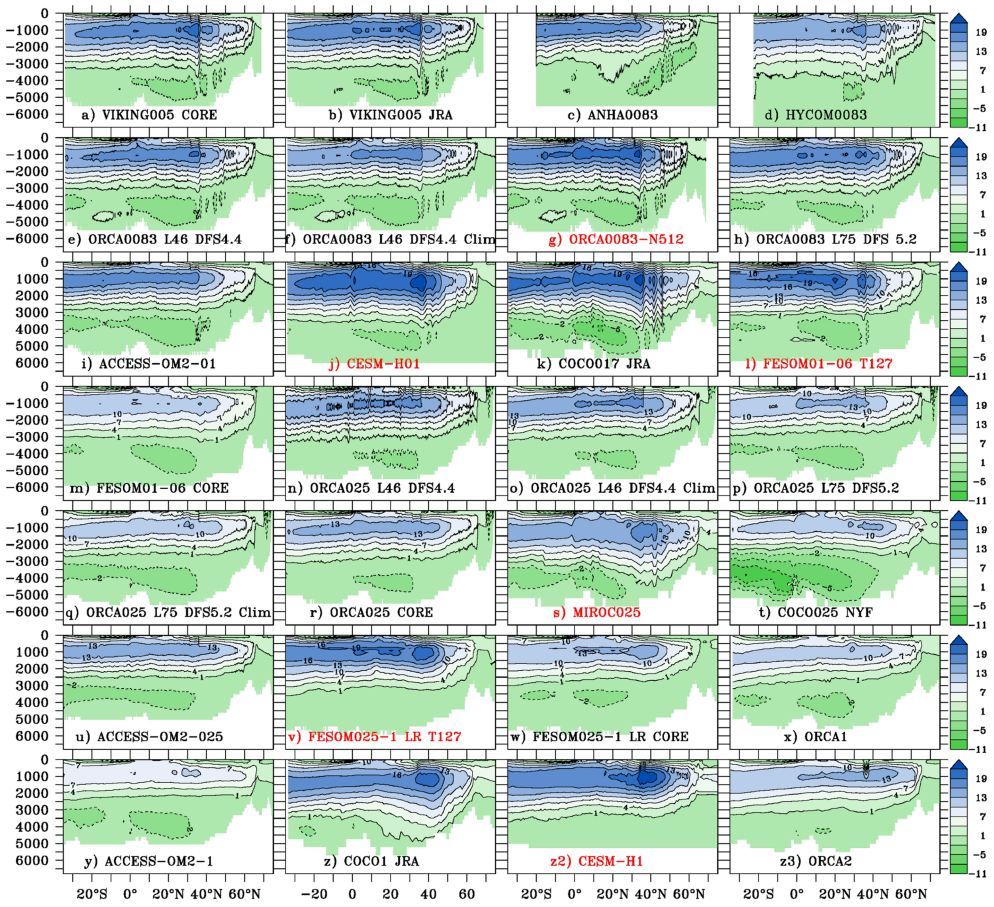

Figure 1. (a–z3) AMOC stream functions in depth coordinates in models from noneddying to eddy-rich simulations. The highest resolutions are shown in the top row and lowest resolutions in the bottom row which are included for comparison. For properties of the models, see Table 1. Coupled ocean-atmosphere models are indicated in red.

A variety of simulations is analyzed to explore the range of AMOC solutions that are possible when mesoscale eddies are represented. We focus on ψ_z in a range of models with resolutions ranging from 1/20° (VIKING) to 2° (ORCA2) (listed in Table 1). Both forced and coupled models are included, and, in some instances, the modeling system is run at different resolutions and/or different surface forcings. Most models are global, but two are configured for the Arctic-North Atlantic (ANHA) or Atlantic-Arctic Basins (VIKING). We also include, in some cases, the low-resolution counterpart to highlight changes that are likely owing to an increase in resolution.

2.1. Dependence of the Mean AMOC on Resolution

The range of solutions for the AMOC is quite broad, and within the eddy-rich models the strength varies by almost a factor of 2 between the strongest and the weakest circulations (Figure 1). Similar results were found for the diversity of mean AMOC by Danabasoglu et al. (2014) in a comparison of low-resolution forced simulations. The strongest AMOC cells are found in the eddy-rich coupled models CESM-H01, FESOM01-06, and ORCA0083-N512. Where comparisons can be made (ORCA0083, FESOM, and MIROC), we also find that the coupled version of the model produces a stronger AMOC than the forced ocean-only configurations. The difference between coupled and uncoupled is most pronounced for FESOM. The reasons why a stronger AMOC is simulated in coupled simulations are not fully understood. However, stronger air-sea interactions with increasing resolution are a plausible cause for stronger AMOC (and of the related meridional heat transport) in high-resolution models (e.g., Grist et al., 2018; Roberts et al., 2016).

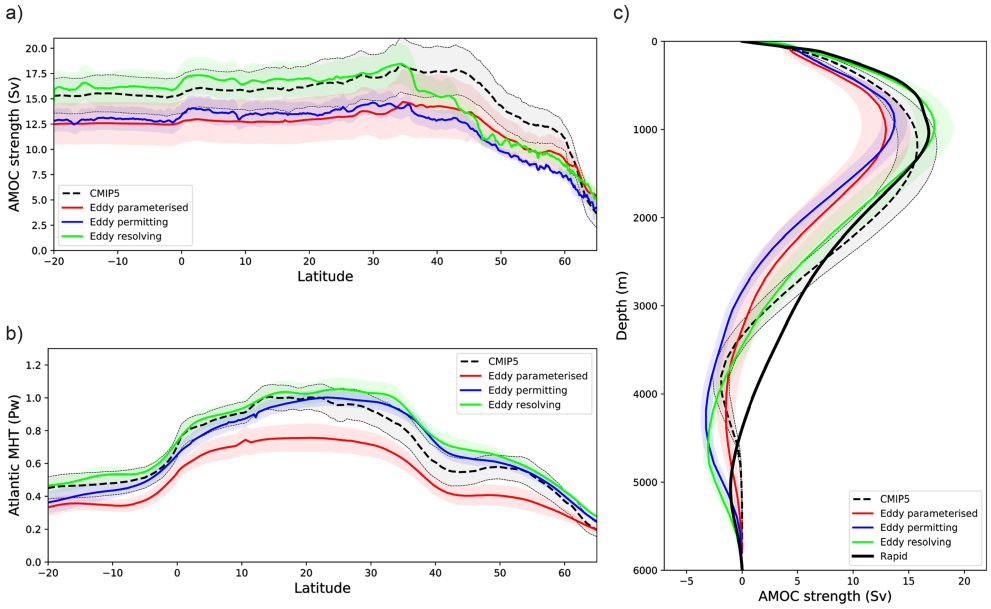

Figure 2. (a–c) Maximum overturning ($\psi(z)$) as a function of latitude for eddy-rich, eddy-permitting, and noneddying models. Solid lines show the average maximum AMOC strength and shading indicates ±0.5 standard deviation. The CMIP5 values included for comparison are based on 29 models: ACCESS1-0, ACCESS1-3, BCC-CSM1-1, BCC-CSM1-1-m, CanESM2, CCSM4, CESM1-BGC, CESM1-CAM5-1-FV2, CESM1-CAM5, CESM1-FASTCHEM, CESM1-WACCM, CMCC-CESM, CMCC-CM, CMCC-CMS, CNRM-CM5-2, CNRM-CM5, CSIRO-Mk3-6-0, EC-EARTH, FGOALS-g2, GFDL-ESM 2G, GFDL-ESM 2M, GISS-E2-R-CC, GISS-E2-R, HadCM3, HadGEM2-AO, HadGEM2-CC, HadGEM2-ES, IPSL-CM5A-LR, IPSL-CM5A-MR, MRI-CGCM3, MRI-ESM 1, NorESM1-ME, NorESM1-M (see, e.g., Mecking et al., 2017 for more details about these models).

Quantitative metrics for AMOC can be defined allowing comparisons among the models (Figure 2). South of about 35–40°N, the maximum overturning strength $\psi(z)_{\max}$ (i.e., the maximum value of ψ occurring in the water column for each latitude) in eddy-rich models is on average about 3–4 Sv stronger than in the eddy-permitting and noneddying models listed in Table 1 (Figure 2a). Between the equator and about 35°N, the AMOC strength is nearly constant with latitude and eddy-rich models simulate the largest AMOC strengths. To a lesser extent, this plateau is also seen for the eddy-permitting models. Between 35–40°N and 50°N, there is a sharp decrease in $\psi(z)_{\max}$ for the eddy-rich models to about 60% of the value at 26°N (Figure 2a). This decrease is a bit less pronounced in the eddy-permitting models and at 50°N $\psi(z)_{\max}$ is about 70% of its 26°N value. A different picture characterizes $\psi(z)_{\max}$ in the noneddying models. On average the maximum AMOC strength also occurs between 25°N and 40°N but the sharp decrease seen for the high-resolution model is not seen at coarser resolution. At 50°N the $\psi(z)_{\max}$ in the noneddying models is still about 90% of its 26°N value and the sharpest decrease in $\psi(z)_{\max}$ occurs north of about 55–60°N (Figure 2b). We will return to this difference between eddy-rich/permitting and noneddying models and its meaning in terms of AMOC pathways in section 3.

To compare with a larger set of low-resolution models, Figure 2 also shows $\psi(z)_{\max}$ obtained from a large subset of 29 models from the Climate Model Intercomparison Project phase 5 (CMIP5). For the CMIP5 models $\psi(z)_{\max}$ is noticeably stronger than for the low-resolution models listed in Table 1. South of about 35°N $\psi(z)_{\max}$ is only marginally lower than for the eddy-rich models. However, the latitudinal dependence of the AMOC strength in CMIP5 models is very similar to that in our set of coarse-resolution models (CMIP5 curve has similar shape but is shifted upward by ~3 Sv). The CMIP5 models show the same behavior as the low-resolution models discussed here, but the average of the 29 models is offset by about 3 Sv from the average of the models discussed here. In the CMIP5 models $\psi(z)_{\max}$ also reach its highest values between about 25°N and 45°N and at 50°N $\psi(z)_{\max}$ is more than 90% of the value at 26°N. It is worth noting here that most CMIP5 models were tuned toward a realistic AMOC strength. No such tuning was done for the high-resolution models presented here. Apart from the horizontal resolution the high and low versions were

kept as similar as possible. This suggests that the sharp decrease in $\psi(z)_{\max}$ between 26°N and 50°N in high-resolution models compared with low-resolution models is a robust feature.

The eddy-rich models have the strongest MHT (meridional heat transport) with the highest values occurring between about 15°N and 35°N (Figure 2b). Only marginally weaker values are found for the eddy-permitting models, while the MHT is clearly lower in low-resolution models. Consistent with $\psi(z)_{\max}$, the MHT is clearly higher in the CMIP5 ensemble than for the low-resolution models listed in Table 1. South of about 20°N, the MHT is very similar in CMIP5 and in the eddy-rich models. North of about 25°N, the MHT is slightly lower than in the eddy-rich models but the differences are not large. For MHT the shapes of the curves are more similar between low- and high-resolution models than for the MOC curves shown in Figure 2a. For latitudes north of about 30°N some CMIP5 models get similar MHT values than eddy-rich models but Figures 2a and 2b suggest that the relative contributions of overturning and gyres are different in the CMIP5 models than in the eddy-rich models and that noneddying models may get the "right" MHT transport for the wrong reason.

Another feature that is apparent is a deepening of the AMOC cell at eddy-rich resolutions compared to the eddy-permitting and noneddying models as defined by the vertical structure of $\psi(z)$ at 26°N (Figure 2c). However, all of the model AMOC cells are too shallow compared to observational estimates (Figures 1 and 2c; Lumpkin & Speer, 2007). Profiles of $\psi(z)$ at 26.5°N where a comparison with the RAPID observations can be made show very good agreement in the top 2,000 m (Figure 2c). However, below 2,000 m the modeled AMOC values are lower than the observation-derived transports, which suggests that the southward return flow of the AMOC simulated at depth is shallower than in observations. However, there is an improvement over the noneddying forced simulations (discussed in Danabasoglu et al., 2014) in the strength of the southward flow. In the CMIP5 models $\psi(z)_{\max}$ at 26°N is too deep but the southward return flow for $\psi(z)$ occurs at depths that are too shallow (indicated by the more rapid decrease of $\psi(z)$ with depth than in the observations or the eddy-rich models). The vertical extent of the AMOC cell looks very similar in z-level models and HYCOM, which uses hybrid coordinates (Figure 1). One could perhaps expect that hybrid coordinates would favor a deeper overturning cell than z-levels but this is not the case here. This result was also seen in the lower-resolution hybrid coordinate model used in Danabasoglu et al. (2014).

There is an indication that the AMOC slightly deepens in the model configurations using a higher number of vertical levels—for example, ORCA0083 with either 46 or 75 vertical levels. The effect is not pronounced though, and it is not clear how robust it is as the coupled version of ORCA0083 (which also used 75 vertical levels) has a marginally shallower AMOC cell than the forced ORCA0083 version. It is worth remembering that the AMOC from RAPID is obtained from density observations and using the thermal wind relation to infer geostrophic velocities. Whereas there is strong evidence that the RAPID approach leads to a good estimate of the "true" AMOC strength and variability (e.g., Hirschi et al., 2013; Sinha et al., 2018), the "true" AMOC could conceivably fall between the models and the AMOC estimate from RAPID.

To illustrate the impact of increasing the horizontal resolution, Figure 3 shows the differences between high- and low-resolution models for $\psi(z)$ where both versions of the model (using the same forcing fields or atmospheric model) are available. The differences between eddy-rich and noneddying configurations all show an increase in the strength of the NADW cell in the eddy-rich models. This is strongest for ORCA and ACCESS with an increase of the overturning cell by up to 8–10 Sv. Smaller increases between 2 and 6 Sv are seen for CESM-H and COCO. The latter also shows a significant increase in the strength of the AABW cell at depth. In COCO the strengthening of the NADW cell is confined to the top 2,000 m, whereas positive anomalies reach down to about 3,500 m for ORCA, ACCESS, and CESM-H. Much smaller differences are found for FESOM (both forced and coupled) where positive anomalies are confined to depths between about 1,500 and 4,000 m. These smaller differences for FESOM are not unexpected since both the high- and low-resolution versions are eddying, that is, eddy rich (FESOM01-06) and eddy permitting (FESOM025-1). A feature which can also be seen in all but one case (ACCESS) is weak negative overturning anomalies north of about 40°N which is consistent with the similar or slightly higher overturning values simulated by low-resolution models at high latitudes (Figure 2a).

It is important to acknowledge that the AMOC strength and vertical structure are very sensitive to surface forcing. The models included in this review do not allow us to systematically assess the influence of the

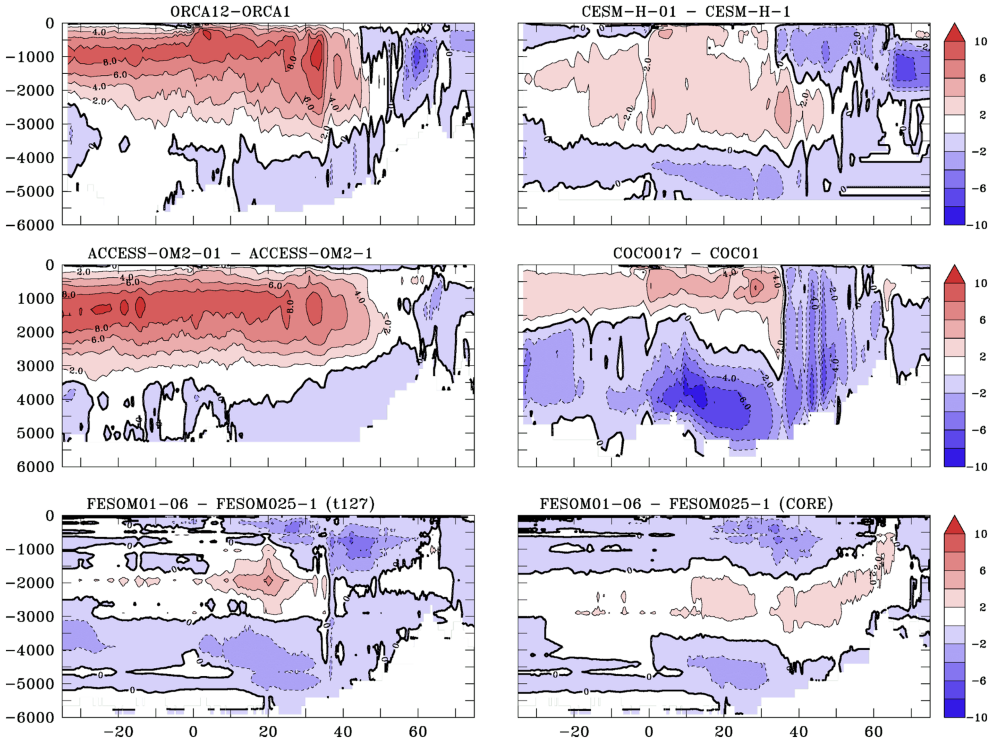

Figure 3. AMOC differences between the high- and low-resolution versions of ACCESS, CESM-H, COCO, and ORCA. Contour interval is 2Sv.

surface forcing. We made opportunistic use of available high-resolution model output, and no attempt was made here to either compare models using the same surface forcing to many different models (e.g., as in Danabasoglu et al., 2014) or to systematically assess the impact of using different surface forcings. Nevertheless, the surface forcing in the models included here (Table 1 and Figure 1) either uses a range of forcings: CORE, DFS, JRA, and CGR over differing time periods or they are coupled ocean-atmosphere models. Forcing differences may explain some of the range of the AMOC solutions. The range of solutions we present here is consistent with earlier studies of both low-resolution (e.g., Danabasoglu et al., 2014) and high-resolution (e.g., Behrens et al., 2013) models.

3. What (Knowledge) Have We Gained?

In this section we highlight key improvements that have been made in the representation of the AMOC as resolution is increased.

3.1. AMOC Pathways

High-resolution ocean simulations have contributed to our understanding of how and on what spatial and temporal scales the AMOC can exhibit variability. Both observations and the models highlight that the picture of a global conveyor belt, a term first coined by Broecker (1987) and subsequently often used to describe the global meridional overturning circulation, is a very much simplified view (Lozier, 2010). The picture of a conveyor as well as that of a meridionally coherent overturning circulation stream function, as illustrated in Figure 1, only emerges when averaging velocities over several years or longer. Any snapshot (or averaging on timescales shorter than about monthly) of the AMOC reveals the much more intricate, complex nature of the ocean circulation. Currents implied to be coherent flows in AMOC schematics can be seen to consist of a succession of eddies and filaments (with some coherent jets in places such as the Gulf Stream between Florida and Cape Hatteras; e.g., Hirschi et al., 2019). For surface currents, this picture is confirmed in both satellite observations and in high-resolution ocean models and for many features there is remarkable agreement between observations and model simulations (Figure 4). In particular the Florida Current and Gulf

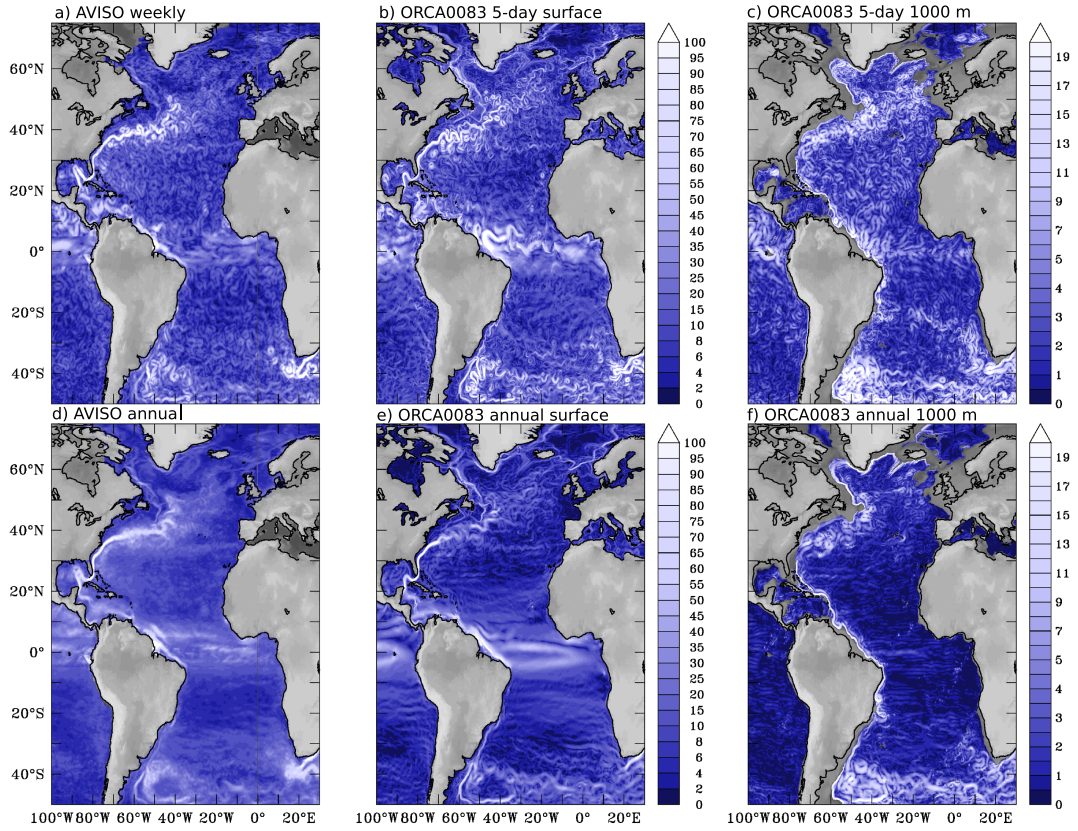

Figure 4. (a–f) Absolute velocities in cm/s from AVISO (geostrophic velocities) and ORCA0083 (ORCA0083-N512). Weekly and annual averages are shown at surface for AVISO (from year 2007); 5-day and annual averages are shown at the surface and 1,000-m depth for the model solution (from model year 2007).

Stream are well represented in the high-resolution simulations with the path of the Gulf Stream separating at Cape Hatteras in high resolution but hugging the coast well past Cape Hatteras in the low-resolution simulations (Chassignet & Marshall, 2008; Danabasoglu et al., 2014). In addition, the path of the North Atlantic Current is qualitatively well represented in the high-resolution simulations. This is thought to be a key region for modulating decadal variability in low-resolution simulations (Buckley & Marshall, 2016).

The eddy-rich circulation is not confined to the surface, but the velocity field at greater depths also shows similarly intricate circulation features (albeit with lower velocities, Figures 4c and 4f). Modeled current velocities reveal interior pathways resembling observations from Lagrangian floats (Figure 4c; Bower et al., 2009, 2011). These interior pathways are thought to be signatures of eddy-driven recirculation gyres (Lozier, 1997, 1999), as shown in both hydrographic data and eddy-permitting and eddy-rich simulations, which represent key routes for the export of Labrador Sea Water into the subtropical North Atlantic (Gary et al., 2011; Lozier et al., 2013). South of the equator, the structure of the DWBC also becomes dominated by eddies (Figure 4c), as observed around 8°S (Dengler et al., 2004), before splitting into two pathways further south, one continuing along the continental shelf and the other spreading in the interior of the basin (Garzoli et al., 2015).

The improvements in the position and strength of currents are reflected in integral quantities as well. The vertically integrated transport of the subpolar gyre (SPG) strongly depends on resolution (Figure 5). In the models used for this review the SPG is stronger at eddy-rich resolutions with maximum values of 30–50 Sv in the Labrador and Irminger Seas with a shape consistent with observations (Treguier et al., 2005; Colin de Verdière & Ollitrault, 2016; Figure 5f). The SPG also extends southward along the coast of North America with a narrow wedge reaching Cape Hatteras, consistent with the separation of the Gulf Stream at Cape Hatteras (Figures 5a–5c). A vigorous SPG is still simulated at eddy-permitting resolution, but the position of the intergyre boundary shifts northward (especially off Cape Hatteras) and the narrow wedge

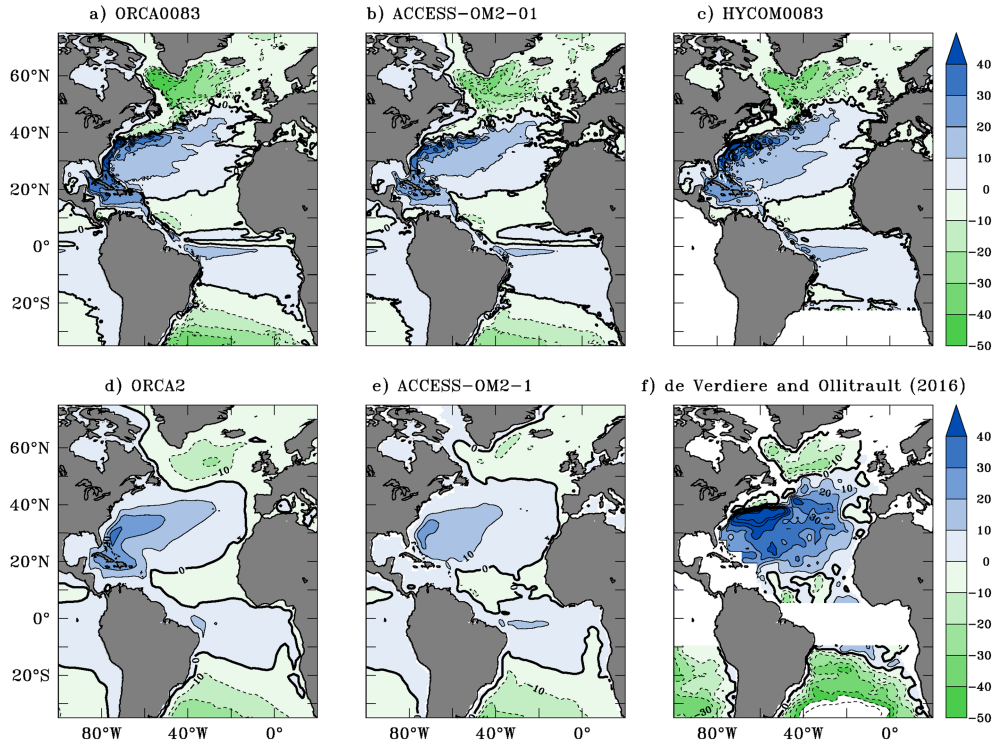

Figure 5. The barotropic stream function in the North Atlantic (Sv) averaged over the last 30 years of the simulations for high and low resolutions: (a) ORCA0083, (b) ACCESS-OM2-01, (c) HYCOM0083, (d) ORCA025, and (e) ACCESS-OM2-1. (f) Barotropic stream function from Colin de Verdière and Ollitrault (2016) inferred from Argo displacements, temperature and salinity climatology, and wind stress.

toward Cape Hatteras disappears (not shown). It is worth noting that Colin de Verdière and Ollitrault (2016) acknowledge that while their approach yields realistic gyre shapes, the quantitative stream function values are likely to be unreliable in the interior of the gyres. Compared to the eddy-rich models, the barotropic stream function of Colin de Verdière and Ollitrault (2016) is weaker in the SPG and stronger in the subtropical gyre.

At noneddying resolutions the SPG is weaker (10–20 Sv maximum) in particular in the western SPG (Figures 5d and 5e). However, only a limited number of low-resolution simulations are used for comparison here. In the literature there are examples of low-resolution models that exhibit vigorous SPG circulations of 30–45 Sv (e.g., Danabasoglu et al., 2014; Yeager et al., 2015). However, as for the AMOC, low-resolution models exhibit a large range of values for the maximum SPG strength (Danabasoglu et al., 2014; their Figure 16) with the majority of models simulating an SPG strength between 15 and about 30 Sv. It is noteworthy that the version of ACCESS (1°, CORE forced) used in Danabasoglu et al. (2014) has a vigorous (~35 Sv) circulation, but in ACCESS-OM2-1 the SPG strength is only 10–20 Sv which suggests a large sensitivity to forcing and parameter choices. Neither of the high-resolution simulations used in this review nor any eddy-rich simulations we are aware of reported a weak SPG circulation—despite different forcings, coupling to different atmospheres, or different parameter choices. This suggests that a vigorous SPG of realistic strength is a robust feature of eddy-rich simulations.

The changes in the representation of the SPG (more realistic currents around Greenland/Labrador and strength) have implications for how currents project on the AMOC in depth and in density coordinates (Figure 6). Only when the zonally integrated meridional flow is nonzero is there a projection onto the AMOC in depth coordinates $\psi(z)$; a gyre circulation with compensating northward and southward flows along its western and eastern flanks does not project onto $\psi(z)$. In density coordinates, both overturning and gyre transports project onto $\psi(\sigma_2)$ as long as compensating volume transports occur in different density classes. The SPG strongly projects onto $\psi(\sigma_2)$ as it is characterized by a large density contrast between the

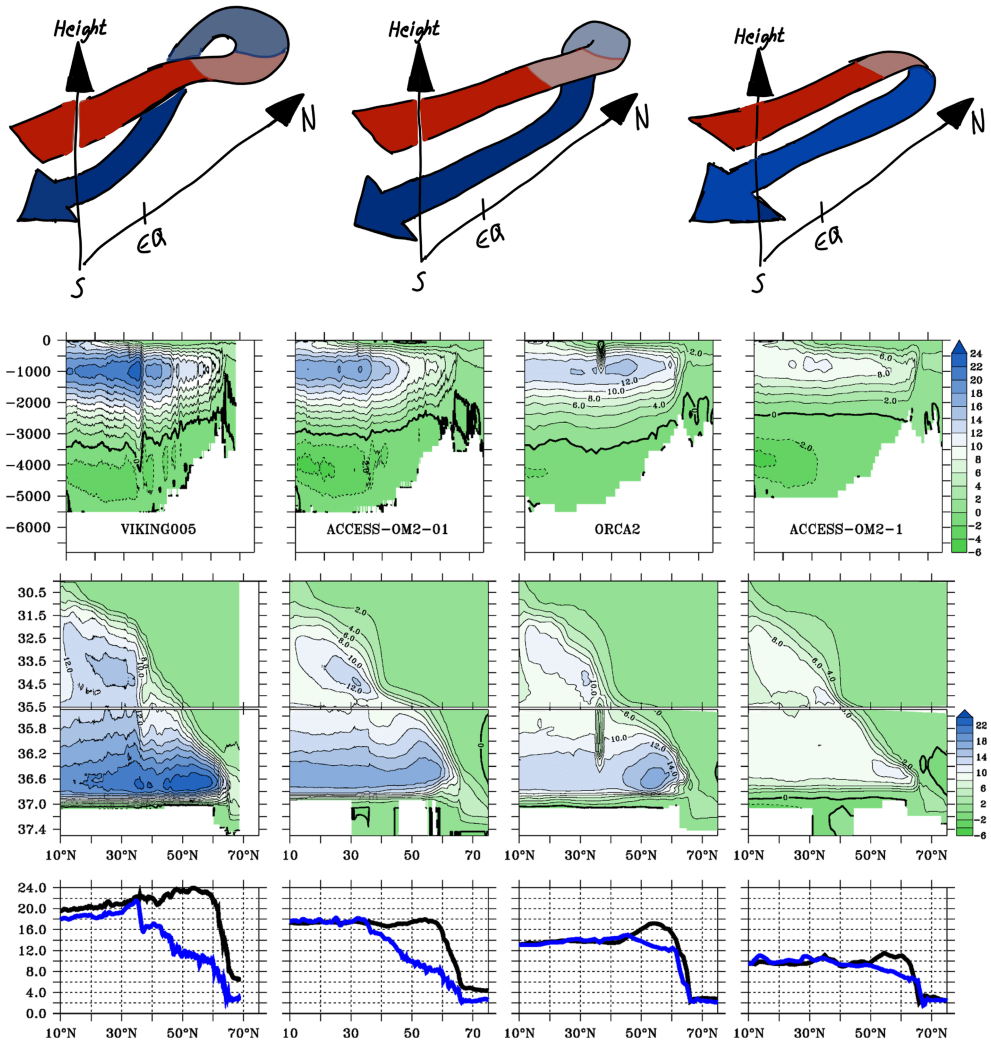

Figure 6. Schematic of main AMOC pathways at high resolution with vigorous SPG (top left), low resolution and weak SPG (top middle) as well as "classic" conveyor-type pathway as expected in, for example, box models (top right) Colors (red to blue) indicate the gradual cooling and density increase of water masses along the AMOC path. AMOC in depth (second row) and potential density referenced to 2,000-dbar (third row) coordinates for two high-resolution (VIKING005, ACCESS-OM2-01) and low-resolution (ORCA2, ACCESS-OM2-1) simulations. Bottom row: maximum values of $\psi(z)$ (blue) and $\psi(\sigma_2)$ (black).

predominantly northward transport in the eastern SPG and the return flow along Greenland and Labrador in the western SPG (e.g., Lherminier et al., 2007).

The AMOC cell in depth coordinates $\psi(z)$ weakens markedly north of about 30–40°N in eddy-rich simulations (illustrated for VIKING005 and ACCESS-0M2-01 in Figure 6). This is indicative of significant sinking between middle and high latitudes. At low resolutions, the sharpest weakening of $\psi(z)$ occurs close to the northern limit of the overturning cell, which is illustrated in Figure 6 for ORCA2 and ACCESS-OM2-1 and Figure 2a. Previous studies have shown similar differences between $\psi(z)$ in high- and low-resolution models (e.g., Treguier et al., 2006; Marsh et al., 2009; Katsman et al., 2018), suggesting that in low-resolution models a larger fraction of the sinking occurs at the northernmost latitudes of $\psi(z)$ in low-resolution models than in high-resolution models.

The weakening of the AMOC cell $\psi(z)$ between middle and high latitudes seen at high resolutions is indicative of a change in the dominant AMOC flow pathways north of about 40–50°N. This can be illustrated by comparing the shapes for the AMOC in depth and in density coordinates (Figure 6). The overturning maximum is consistently found at higher latitudes for $\psi(\sigma_2)$ than $\psi(z)$, but this difference is more pronounced at

high than at low resolution (Talandier et al., 2014). This is consistent with the stronger SPG simulated at high resolution, with warm and salty waters from the North Atlantic Current flowing northeastward and forming the eastern flank of the SPG. These waters are less dense than the colder, fresher southward flowing waters along Greenland and the Labrador Shelf in the western SPG.

The stronger SPG and more realistic current pathways at high resolutions means that these transports of contrasting water masses project strongly on $\psi(\sigma_2)$. The highest values of $\psi(\sigma_2)$ occur between about 50°N and 60°N in high-resolution models (Figure 6, columns for VIKING005 and ACCESS-OM2-01), and $\psi(z)$ is only about half the strength of $\psi(\sigma_2)$. In contrast, at low resolution the maximum values for $\psi(\sigma_2)$ are reached at similar latitudes as found in high resolution, but at these latitudes $\psi(z)$ in low resolution is 70–80% of $\psi(\sigma_2)$. The low-resolution versions of VIKING/ORCA (NEMO) and ACCESS-OM2 have a weaker SPG when compared to other low-resolution models. However, a strong SPG in a low-resolution model does not necessarily mean high subpolar values for $\psi(\sigma_2)$. Low-resolution models (e.g., Danabasoglu et al., 2014; Zhang, 2010) consistently show a smaller difference between $\psi(z)$ and $\psi(\sigma_2)$ north of about 30°N than for the high-resolution examples shown in Figure 6 (or in other studies such as Grist et al., 2012). In Zhang et al. (2010) the maximum MOC strength, in this low-resolution simulation with a relatively strong SPG, is only marginally weaker in depth (20–22 Sv) than in density coordinates (24 Sv) and the latitudes where the highest AMOC values occur overlap. The same is true for the larger low-resolution model ensemble studied in Danabasoglu et al. (2014) where the results show that the values of $\psi(z)$ are at least 70–80% of those seen for $\psi(\sigma_2)$ between about 40°N and 60°N (comparing their Figures 3 and 4). In the examples shown in Figure 6 it is only north of about 50°N that the maximum values of $\psi(\sigma_2)$ and $\psi(z)$ diverge at low resolution, whereas differences start at about 35°N for the eddy-rich models (Figure 6, bottom). For the high-resolution models the values of $\psi(z)$ between 40°N and 60°N are only about 50% of $\psi(\sigma_2)$ suggesting a stronger gyre contribution to $\psi(\sigma_2)$.

The impact of the difference in the pathways between high- and low-resolution models and their impact to the AMOC are illustrated in Figure 5. For very coarse, 2-D models or box-models, the AMOC circulation is close to the "classic" conveyor type with water masses moving northward, sinking (over a relatively small range of latitudes) and returning south at depth. At coarser, noneddying resolution, the AMOC no longer purely consists of its overturning component. There is also a weak gyre contribution symbolized by a little loop at the northern end of the conveyor schematic (Figure 5). At high resolution, there is a clear horizontal loop at high latitudes symbolizing a vigorous SPG (which projects on $\psi(\sigma_2)$ but not $\psi(z)$). This change in pathways is also linked to changes in the location of the sinking. Whereas at low resolutions sinking occurs mainly in the central Labrador and Irminger Seas, it is concentrated along the northern and western flanks of the SPG at eddy-permitting resolutions (Katsman et al., 2018).

3.2. AMOC Variability and Stability

Since 2004 AMOC observations at 26°N have shown variability on timescales ranging from submonthly up to what we have observed (e.g., Smeed et al., 2018). From models and observations we know that the AMOC likely varies on subdaily to millennial timescales and longer. In this section we will focus on aspects of the AMOC variability and AMOC features that have either been first described in high-resolution models or studies in which high-resolution models have shed new light. For more general discussions on the AMOC variability and on the underlying mechanisms the reader is referred to Buckley and Marshall (2016).

3.2.1. Overview of Subdaily to Decadal AMOC Variability

The AMOC variability found in high-resolution models on different timescales is illustrated with the standard deviation of the overturning $\psi(z)$ (Figure 7). By far the largest variability occurs on the shortest timescales (subdaily to daily). We note that seeing the highest variability on short timescales is not specific to high-resolution models; this is true for low-resolution models as well. However, especially on very short timescales (subdaily to perhaps weekly) high-resolution models have been shown to exhibit AMOC variability which has not been reported from low-resolution models (e.g., Blaker et al., 2012). Additionally, the presence of eddies adds chaotic-intrinsic variability on a range of timescales which is not present at low resolution (e.g., Hirschi et al., 2013; Grégorio et al., 2015; Leroux et al., 2018; see also section 3.2.2). The highest standard deviations of 40–50 Sv are centered within a few degrees of latitude around the equator. Standard deviation values away from the equator are much lower albeit still substantial (maximum of 7–8 Sv). This latitudinal variability structure is maintained when the AMOC variability is

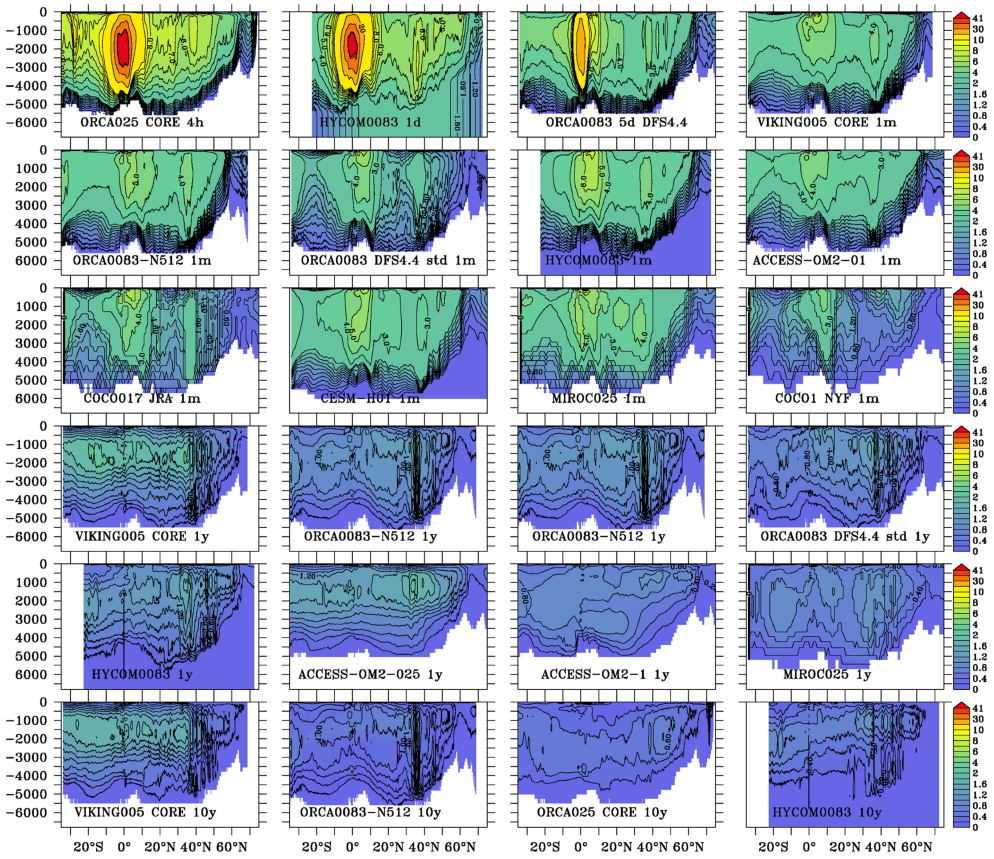

Figure 7. Standard deviation of AMOC (Sv) across a range of models. The standard deviations shown are computed from 4-hourly, daily, 5-daily, monthly, yearly, and decadal averages. The panels are arranged with the variability obtained from the highest temporal resolution (top left, 4-hourly) to the lowest temporal resolution (bottom row, 10 years). Between 0 and 2 Sv the contour interval is 0.2 Sv, from 2–10 Sv it is 1 Sv, and from 10–40 Sv it is 10 Sv.

computed from daily or 5-day averages, but the maximum values reduce to about 20 and 5 Sv at equatorial and extraequatorial locations. For the timescales of up to 5 days the depth of the maximum variability is around 2,000 m for most latitudes. The pronounced equatorial variability maximum disappears when using monthly or longer timescales, but the largest variability still occurs in the equatorial region with values of about 5–6 Sv. However, these values no longer stand out as clearly compared to the maximum values of 3–4 Sv found away from the equator. The equatorial maximum is no longer seen when the variability is computed from annual means, and the largest values of 1–2 Sv are now seen in the North Atlantic between 20°N and 50°N. This meridional variability structure remains broadly similar when computing the AMOC variability from decadal means, but the values are reduced with maxima of about 1 Sv.

The presence of large AMOC variability in high-resolution ocean models has been known for a number of years. In fact, models suggested the presence of a large (peak-to-peak of more than 10 Sv within a few months) midlatitude AMOC variability on subannual to interannual timescales (e.g., Baehr et al., 2004; Hirschi et al., 2003) before the first direct AMOC observations confirmed that variability of that magnitude exists in the real ocean (Cunningham et al., 2007; McCarthy et al., 2012). Models also suggested that westward propagating features are not only key to the adjustment of the long-term basin-wide density gradients but that they can also cause subannual to interannual fluctuations of basin-wide zonal density (and pressure) gradients that project onto the geostrophic component of the AMOC (e.g., Köhl, 2005; Hirschi et al., 2007; Cabanes et al., 2008). A particular benefit from models is the ability to use them to study how local AMOC estimates (i.e., across given sections as in RAPID or OSNAP) can be interpreted in a wider spatial context (Biastoch et al., 2008; Bingham et al., 2007; Hirschi et al., 2013). Although this

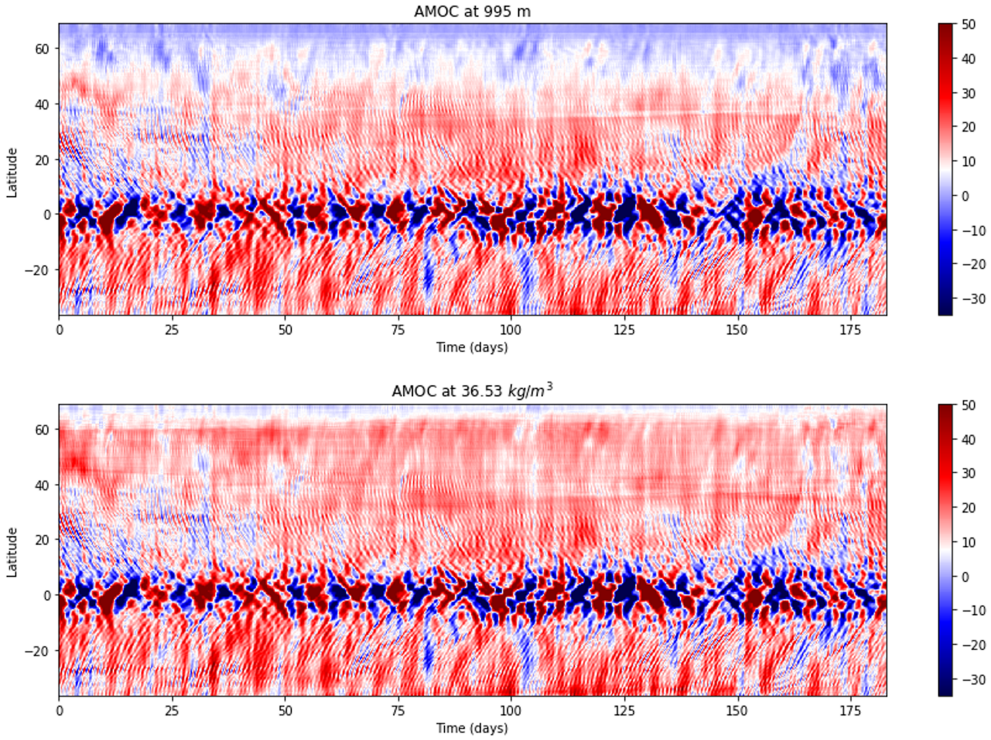

Figure 8. Hovmoeller diagram of $\psi(z)$ at 995-m depth (top) and $\psi(\sigma_2)$ at 36.53 kg/m3 (bottom) as a function of time and latitude from 4-hourly averages in an ORCA025 simulation. Units are Sv.

can also be done using low-resolution models, high resolution is desirable because at low resolution boundary waves mediating AMOC changes are poorly represented due to poor representation of the continental shelf and key currents such as western boundary currents are too diffuse with velocities that are too low.

A recent interesting aspect revealed in high-resolution ocean simulations is the suggested presence of previously unknown types of AMOC variability. The very high AMOC variability found on subdaily timescales (Figure 7) was initially unexpected but was subsequently shown to be caused by the passage of near-inertial waves triggered by wind variability at middle to high latitudes (Blaker et al., 2012). The magnitude of this AMOC variability is large (e.g., standard deviation of 7–8 Sv and peak-to-peak of up to 50 Sv at 26°N). To date, no observations exist to confirm the existence of such a near-inertial AMOC variability in the real ocean. However, near-inertial gravity waves are known to be ubiquitous in the world ocean and their presence has been confirmed by numerous observations (e.g., Alford, 2003; Alford et al., 2016). They have also been simulated in different ocean models (Fox et al., 2000; Komori et al., 2008), and theoretical considerations suggest that the AMOC may have a resonance at near-inertial timescales (Sevellec et al., 2013). Whether near-inertial gravity waves do indeed project onto the AMOC in nature is not yet known. What we can say, though, is that if they do exist in nature, then these AMOC oscillations would be invisible to the RAPID (or OSNAP) observing systems. The near-inertial impact on the AMOC is found in the nongeostrophic component, and direct velocity measurements across the full sections would be required to capture it.

Even larger variability (peak-to-peak of 400 Sv, standard deviation >50 Sv) has been found around the equator (Hirschi et al., 2013). The dominant timescales of these oscillations are between 5 and 10 days, and they are caused by the wind variability in the equatorial region projecting onto baroclinic modes linked to equatorially trapped near-inertial waves. Similar to the near-inertial AMOC oscillations mentioned earlier (Blaker et al., 2012), there is no observational evidence yet that such a high equatorial variability exists in nature. However, the mechanisms through which this high-frequency AMOC variability occurs in high-resolution ocean models are known to exist, even if it is currently unknown whether they can project onto the AMOC as strongly as the models suggest. Even in models, it is currently unclear whether these large

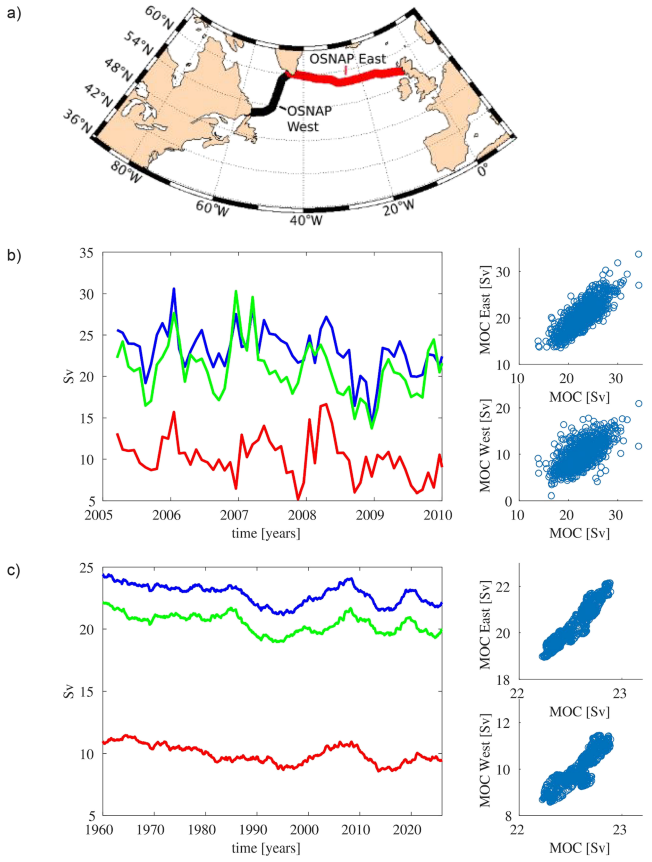

Figure 9. (a) Location of the eastern and western parts of the OSNAP section. (b) Left: maximum AMOC transports (MOC east/west) across the western and eastern OSNAP sections in ORCA0083-N512 (control simulation). Shown is the AMOC across the full OSNAP section (blue), the western (red), and eastern (green) parts of the section. Right: MOC east versus MOC (top) and MOC west versus MOC (bottom). The time series are shown for the last 8 years of the simulation, and the scatter plots show monthly values for the 76 years of the simulation (1950 to 2026). (c) Same as (b) but for the whole length of the simulation and for transport filtered with a 5-year running average. Note that (as in OSNAP) different densities are used for the western, eastern, and full sections. Therefore, the sum of the eastern and western transport is not equal to the transport for the full section.

high-frequency AMOC oscillations play a role on climate timescales. It is conceivable that they could enhance vertical mixing and hence affect the mean ocean state (and mean AMOC strength). However, at this stage it is equally possible that these oscillations—even though very large—are just "sloshing" water around without much interaction with the mean circulation and little consequence for climate. Note that these high-frequency AMOC features project on both $\psi(z)$ and $\psi(\sigma_2)$ (Figure 8). Numerous observational studies show that near-inertial gravity waves are ubiquitous in the ocean (e.g., Alford et al., 2016), and sea surface height variability shows variability on timescales consistent with the large equatorial AMOC variability (Durland & Farrar, 2012; Farrar & Durland, 2012) so the large high-frequency AMOC variability simulated in high-resolution ocean models may well be real. This is illustrated using output from an ORCA025 simulation where 4-hourly averages are available for a 6-month period. The presence of a clear variability signal in $\psi(\sigma_2)$ suggests that, even if not yet demonstrated, an impact on diapycnal mixing is plausible.

3.2.2. Eastern Versus Western Subpolar AMOC Variability

An important feature of the AMOC was recently revealed by the OSNAP observations in the subpolar North Atlantic. The AMOC estimate obtained from the first 21 months of observations from the OSNAP line suggests that the largest fraction of the AMOC variability on monthly timescales originates from the eastern part of the section with little AMOC variability coming from the Labrador Sea (Lozier et al., 2019). This time series provides a new benchmark against which we should test models. Many previous studies have looked at the importance of the Labrador Sea on the AMOC and its variability (e.g., Böning et al., 1996, 2006; Pickart & Spall, 2007; Robson et al., 2014; Rahmstorf et al., 2015; Feucher et al., 2019). What emerges from these studies is the likely importance of Labrador Sea processes for the AMOC and its variability on decadal or longer timescales. However, a recent analysis by Li et al. (2019) revealed that ocean models at eddy-permitting resolution and coarser are generally biased by an overproduction of Labrador Sea Water compared to observations, which tends to strengthen the AMOC response to changes in the volume of this water mass. Furthermore, the relationship between AMOC and Labrador Sea Water properties was found to degrade considerably downstream of the basin (Li et al., 2019).

In the context of this review, we examine the respective contributions from the eastern and western parts of the OSNAP sections in one of the latest coupled high-resolution models (ORCA0083-N512). As in OSNAP, the transports are calculated in density coordinates and the AMOC is split into an eastern and western AMOC (Figure 9a). The transports shown are either monthly averages (Figure 9b) or smoothed with a 5-year running average (Figure 9c). For monthly values the amplitude of the variability is similar for the eastern and western subpolar North Atlantic. Both the eastern and western AMOC transports are significantly correlated with the total subpolar AMOC, but the correlation is stronger for the eastern AMOC ($r = 0.81$) than for the western AMOC ($r = 0.65$). This means that a larger fraction (65%) of the variance has its origin in the eastern subpolar North Atlantic, but the variability contribution from the Labrador Sea is far from negligible (42% of variance). The 21-month record presented in Lozier et al. (2019) shows almost no AMOC variability originating from the western part of the section. Nevertheless, the model supports the view that the AMOC contribution from the eastern subpolar North Atlantic plays an important role in the total AMOC variability. The model time series are much longer than the observational record (21 months). Figure 9c shows that a high correlation between the eastern AMOC transport and the total AMOC is maintained on decadal timescales with correlations similar between the total AMOC and the eastern and western transports (both >0.9). The model simulation suggests that

based on monthly values, the dominance of the east Atlantic on the subpolar AMOC variability is found throughout the simulation (Figure 9b), but on decadal timescales both eastern and western transports contribute approximately equally to the total AMOC (Figure 9c). Such analysis suggests that the respective contributions from eastern and western subpolar North Atlantic to the total AMOC should form a routine model performance metric (as, e.g., the AMOC at 26.5°N), calculated on a variety of timescales.

3.2.3. Chaotic/Intrinsic AMOC Variability

In the early days of RAPID AMOC observations, concerns were raised that the variability in the AMOC observations from RAPID could essentially consist of noise related to ocean mesoscale eddies and that "Real-time detection of secular changes in the oceanic overturning circulation by regional measurements is probably a mirage" (Wunsch, 2008). Subsequent observation-based studies did show that the noise level is much lower than what Wunsch (2008) suggested (Kanzow et al., 2009) and that the signal-to-noise ratio is much more favorable to the detection of long-term trends in the AMOC by observing its evolution at one latitude. Nevertheless, AMOC observations show that the AMOC variability on short timescales is large and mesoscale features contribute to this variability.

Mesoscale eddies are the most intense and best known source of chaotic/intrinsic variability in the ocean: their phase is indeed inherently random and they spontaneously emerge in the ocean under steady forcing. Mesoscale kinetic energy peaks at relatively small time and space scales as eddies develop, but their mutual interactions subsequently feed chaotic fluctuations at larger space and timescales through spatial and temporal inverse cascades (Arbic et al., 2014; Sérazin et al., 2018). Other nonlinear processes such as large-scale baroclinic instability, distinct from those occurring at the mesoscale, may also coexist with mesoscale instabilities (Huck et al., 2015) and feed multidecadal ocean chaotic variability with a substantial impact on the AMOC (Sévellec & Fedorov, 2013).

A systematic quantification of the impacts of atmospheric variability and intrinsic/chaotic processes on the AMOC variability is very difficult to obtain from observations alone. Different strategies using eddy-permitting/rich simulations have been proposed to quantify these two impacts. Biastoch, Böning, and Lutjeharms (2008), for instance, compared two global simulations where eddies were (i) unresolved everywhere and (ii) resolved in the Agulhas region via a local grid refinement. The results show that resolving eddies in the Agulhas region triggers the emergence of a chaotic/intrinsic AMOC variability reaching interannual to decadal timescales and extending far into the North Atlantic. However, this local grid refinement did not allow nonlinear processes to generate chaotic/intrinsic AMOC variability at other latitudes of the Atlantic. The features and contribution of chaotic/intrinsic AMOC variability emerging in fully turbulent basins have been studied by forcing global ocean models at 2°, 1/4°, and 1/12° resolution by a repeated seasonal atmospheric forcing devoid of any interannual variability (Grégorio et al., 2015). Almost no interannual AMOC variability spontaneously emerged in the laminar 2° simulation, but a large amount of chaotic/intrinsic variability emerged at 1/4° and 1/12°, with comparable imprints on the AMOC. This chaotic/intrinsic AMOC variability was shown to reach multidecadal timescales and the scale of the Atlantic and to account at 35°S for half of the interannual-to-decadal variability found in fully forced hindcasts (simulations driven by the full range of atmospheric timescales—i.e., via an atmospheric reanalysis).

Estimating the relative contributions of the chaotic/intrinsic processes and of the atmospheric variability in the AMOC variability requires ensemble ocean simulations, where all members are driven by the same atmospheric conditions but are started from different initial conditions (as done by, e.g., Hirschi et al., 2013; Penduff et al., 2014; Bessières et al., 2017; Leroux et al., 2018). Note that the different eddy fields between ensemble members mean that air-sea fluxes will also differ as they depend on the local ocean conditions.

Small perturbations to the initial conditions are sufficient to cause the AMOC variability to diverge between different ensemble members. This behavior is illustrated in Figure 10 for the spread of the AMOC at 26.5°N in a small ensemble performed with ORCA0083 forced with interannual data from DFS5.2. A six-member initial condition perturbation ensemble of NEMO ORCA0083, created by advancing the simulation restart by one to five model time steps, shows how the AMOC at 26°N, 1,000-m depth, diverges under identical atmospheric conditions. (Figure 10). Note that as the eddy field diverges between ensemble members, air-sea fluxes will also diverge as the different eddy fields change the local ocean conditions. The ensemble begins on 1 April 2009, from the control simulation. The initial condition perturbations are very small,

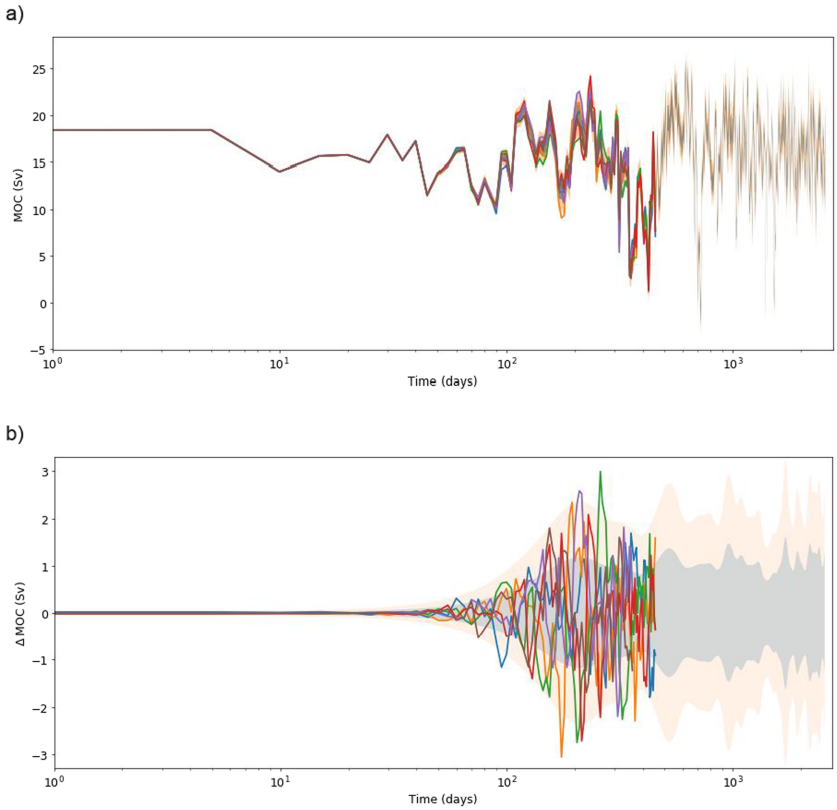

Figure 10. (a) Time series of the 5-day mean AMOC at 26°N and 1,000-m depth for a six-member NEMO ORCA0083 ensemble. Start of all ensembles is 1 January 2009. Two ensemble members cover 1 year (January 2009 to December 2009) and four ensemble members cover 5 years (January 2009 to December 2014). (b) Deviation of the AMOC from the ensemble mean (Sv). The shaded regions in both panels indicate 1 and 2 standard deviations. For clarity, individual members are not plotted beyond 18 months.

and the model AMOC does not diverge for around 30 days. Between 30 days and 6 months, the ensemble diverges. All ensemble members broadly follow the same evolution, and the same dominant peaks and troughs occur in each ensemble member (Figure 10a). However, there is a spread of the AMOC time series around the ensemble mean. This spread is smaller than the variability in the ensemble mean (Figure 10a). The differences from the ensemble mean show that after 6 months the ensemble spread reaches saturation, with a (time mean) standard deviation of 1.1 Sv (Figure 10b). This is 27% of the standard deviation of the ensemble mean (4.15 Sv) which is consistent with Hirschi et al. (2013) (who also used 5-day averages) and Grégorio et al. (2015) and Leroux et al. (2018) (who used monthly and annual averages). In this case the ensemble spread can be interpreted as the contribution of chaotic/intrinsic processes (including mesoscale eddies and larger chaotic anomalies) to the AMOC variability, and the temporal variability of the ensemble mean AMOC provides the atmospherically forced variability. These ensemble statistics confirmed that most of the chaotic AMOC variance remains strong up to multidecadal scales and that the phase of the broadband AMOC fluctuations around the ensemble mean remained random between each ensemble member (Leroux et al., 2018). In other words, the atmospheric variability only paces part of the AMOC fluctuations, while a significant part of the interannual-to-decadal AMOC variance conserves its chaotic character under a reanalyzed forcing. About 50% of the AMOC at 35°S is chaotic/intrinsic falling to typically 20–30% in the North Atlantic up to about 40°N and less than 10% in the subpolar region (Grégorio et al., 2015; Hirschi et al., 2013; Leroux et al., 2018). The reasons for these differences are far from understood yet, but the ensemble simulation strategy can provide some insight into the chaotic/intrinsic processes driving the AMOC fluctuations and into the atmospherically forced origin of certain AMOC anomalies observed in the RAPID time series or elsewhere (Leroux et al., 2018). However, given their large computational cost, large-ensemble global simulations have only been

performed at the coarser end of eddying resolutions (Bessières et al., 2017) or with small ensemble sizes and over short integrations (Figure 10). They nevertheless demonstrate that observed AMOC fluctuations cannot be only attributed to atmospheric forcing. The "eddy noise" propagates to much larger spatiotemporal scales, and as a result the predictability of the AMOC should be reevaluated in the presence of intrinsic ocean turbulence. However, in coupled simulations, eddies can be partly damped by atmospheric fluxes and as a result, eddy variability tends to be larger in forced models (Ma et al., 2016). Furthermore, intrinsic coupled climate variability from processes such as El Niño is also present in coupled models that can create additional low-frequency variability.

3.2.4. AMOC (Bi)stability

One of the key questions in AMOC research, namely, whether the AMOC can exhibit multiple stable states under identical surface boundary conditions, emerged from an analytical 2-box model (Stommel, 1961). Since then the possible existence of multiple AMOC states, the likely conditions required for such multiple states to exist and for the AMOC to rapidly transition from one state to another in the real world, has been at the center of many studies. Multiple states have been obtained in wide range of available models: from analytical models (e.g., Marotzke et al., 1988; Longworth et al., 2005) to complex three-dimensional ocean-only (e.g., Deshayes et al., 2013) and coupled models (e.g., Hawkins et al., 2011; Jackson & Wood, 2018; Manabe & Stouffer, 1988; Mecking et al., 2016). Despite such efforts, we can still not conclusively answer whether multiple AMOC states (and in particular rapid transitions between these states) and related AMOC hysteresis could exist in the real world (e.g., Gent, 2013, 2018; Stocker, 2013). The possibility that the AMOC may have more than one equilibrium, and that a transition to this other equilibrium could be triggered by a large enough perturbation (e.g., a fresh water pulse from the Greenland ice sheet e.g. Weijer et al., 2012), has been a key research question for climatologists for decades; a collapse of the AMOC would have significant climate implications, with large societal repercussions. Despite the potentially high impact, there is still significant uncertainty in the likelihood of such an event (see Weijer et al., 2019 for a review).

Models with low resolutions such as those used in CMIP5 suggest a low probability for an AMOC shutdown under global warming scenarios (Collins et al., 2013). However, it has been suggested that systematic biases in the salinity distribution of the Atlantic may overestimate the stability of the AMOC in these models (Liu et al., 2017; Mecking et al., 2017). A critical argument revolves around a metric called Fov, which is the freshwater flux across 34°S in the South Atlantic due to the AMOC. In most low resolution models the AMOC imports freshwater into the Atlantic (Fov $>$ 0), which would constitute a negative, stabilizing feedback (the so-called salt advection feedback; e.g., Rahmstorf, 1996) on the strength of the AMOC: A weakening of the AMOC would reduce the freshwater import, salinifying the Atlantic, hence resisting a further weakening. Observations, however, suggest that the Fov $<$ 0 at 30°S (e.g., Bryden et al., 2011; McDonagh & King, 2005; Weijer et al., 1999), which would suggest a positive, destabilizing feedback. Several model studies (e.g., de Vries & Weber, 2005; Weber & Drijfhout, 2007) show a surprising ability of the sign of Fov to predict whether the AMOC is in a regime of multiple equilibria (Fov $<$ 0) or not (Fov $>$ 0). Other studies (e.g., Dijkstra, 2007; Huisman et al., 2010) have refined this metric by including the AMOC-induced freshwater transports at the northern boundary of the Atlantic, hence proposing a divergence indicator, Σ Fov. However, caution is warranted in interpreting the negative sign of Fov (or Σ Fov) in observations as a sign of AMOC bistability. For one, the validity (or accuracy) of Fov as a stability indicator has been questioned, as modeling studies suggest that the freshwater transport by the wind-driven gyre circulation may be at least as important as that of the AMOC in shaping the transient response to a large freshwater perturbation (Thomas & Fedorov, 2019; Gent, 2018; Mecking et al., 2016; Spence et al., 2013). But the more relevant question for this review is whether the AMOC stability paradigm—and the role of Fov—carries over from eddy-parameterized to eddy-rich models.

It is encouraging that high-resolution models appear to simulate the correct sign of Fov at 30°S (Deshayes et al., 2013; Mecking et al., 2016). This would give credence to the suggestion that the Fov in low-resolution models is biased positive due to model errors or poorly resolved processes (e.g., Agulhas Leakage; Weijer & Van Sebille, 2014). Experimentation with eddying models should reduce concerns that the stability of the AMOC is compromised by biases in the salinity field.

But one question that needs to be addressed is whether the salt advection feedback, which is a critical ingredient for AMOC bistability, is active and effective in high-resolution models. If this feedback is somehow

incapacitated, or made moot by more powerful feedbacks, then the bistability regime may disappear. For instance, if the meridional coherence of the AMOC is reduced in eddying models, then AMOC changes in the North Atlantic may not be able to affect the freshwater transport across 34°S. Similarly, if an improved representation of air/sea interactions strengthens atmospheric feedbacks like ITCZ shifts, this may have a stronger impact on the freshwater budget than Fov. Mecking et al. (2016) conclude that, in their eddy-permitting model, the salt advection feedback is strengthened by the improved representation of eddies and boundary currents in their eddy-permitting model and that it is still able to stand its ground despite powerful atmospheric feedbacks. But more investigations with eddy-rich models are required to provide a definitive answer as to the effectiveness of the salt advection feedback.

In addition, there are questions even on a more fundamental level. Studies such as Wolfe and Cessi (2014), Wolfe and Cessi (2015), or Mashayek et al. (2015) have shown that the dynamics of an adiabatic overturning circulation are significantly different than those of a diffusive AMOC. Nevertheless, the model of Wolfe and Cessi (2014) and Wolfe and Cessi (2015) is able to simulate a regime of multiple equilibria, with a central role for the salt advection feedback, despite notably different dynamics and a "collapsed" AMOC state that is markedly different from those in low-resolution models (see also Hofmann & Rahmstorf, 2009). So the question is, whether the presence of multiple equilibria is a fundamental aspect of the AMOC in nature and whether our intuition gained from decades of experience with low-resolution models carry over to eddy-rich models. In other words, can we expect, for instance, that Fov is still a valid predictor of bistability in eddying oceans (despite its caveats)? Or is the paradigm shift from diffusive to adiabatic overturning too disruptive, and do we need to reprogram our intuition based on experimentation with eddying models?

It is clear that perturbation experiments with strongly eddying models are needed to establish whether or not eddying and noneddying models display corresponding behavior in terms of bistability.

3.3. Design of Observing Systems

A practical aspect where high-resolution ocean models have proven to be very useful is the testing of possible observational strategies for the AMOC. Their ability to resolve key circulation features makes them ideal testbeds to assess whether a given observational strategy is likely to work or not. This approach has been quite extensively used prior to the deployment of the AMOC observation array at 26.5°N (e.g., Rayner et al., 2011). One can deploy "pseudo" moorings in a model which are subsampling the model ocean in a way that mimics how moorings would sample the real ocean and then reconstruct the AMOC from the pseudo mooring data. Such reconstructions can then be compared against the AMOC in the models, thus providing valuable insights into the advantages and limitations of a chosen observational approach. For the RAPID AMOC observation program, carrying out model tests was a crucial part of the successful bid to continuously observe the AMOC for the first time by measuring temperature and salinity at key locations across the Atlantic at 26.5°N (Baehr et al., 2004; Hirschi et al., 2003). Similar model-based tests have been carried out for other latitudes in the Atlantic to test the feasibility of the AMOC monitoring system SAMOC in the South Atlantic using hydrography moorings and pressure inverted echo sounders (PIES) and hydrography (Perez et al., 2011). Stepanov et al. (2016) use a 1/16° version of NEMO to test the potential to observe the AMOC at 41°N and links between that latitude and 26.5°N. High-resolution ocean models have also been used to demonstrate that the AMOC can be observed by measuring the bottom pressure along the western boundary (Bingham & Hughes, 2008), and such model tests were the foundation for the WAVE array deployed in the North Atlantic between 2004 and 2008 (Elipot et al., 2014).

It is important to note that testing an AMOC observing strategy in a model cannot replace expert knowledge of the local hydrography and bathymetry in the real ocean when it comes to the deployment of instrumentation. For example, even at resolutions of 1/12° (e.g., Sinha et al., 2018) or 1/16° (Stepanov et al., 2016) a pseudo mooring at 26.5°N is a water column with a footprint of 8.3 km × 8.3 km or 6.2 km × 6.2 km with a limited number of vertical levels. Hence, it is clear that results from a model have to be taken only as indicative of whether a method is likely to work in the real ocean and can only serve as a rough guide as to where instruments should be positioned. Nevertheless, when used carefully, models are a powerful tool to assist in the early development stages of observational programs. In a later stage they can also help to gain a better understanding of the limitations of a given observational approach, such as the likely impact of ageostrophic contributions to the AMOC at 26.5°N (Sinha et al., 2018).

4. Areas in Need of Improvement

The following provides an overview of features that even high-resolution models are currently unable to simulate correctly. As illustrated in Figure 1, simulating the AMOC with high-resolution (eddy-rich) models leads to a wide range of solutions for the AMOC. Both in forced and coupled modes the AMOC strength simulated at high resolution is stronger than at lower resolutions and the high-resolution simulations compare more favorably with the AMOC strength observed at 26.5°N. However, the AMOC cell is consistently too shallow compared with observations. This bias holds for the overturning cell as a whole where observational estimates suggest a deeper reaching AMOC cell (Lumpkin & Speer, 2007; Talley et al. 2007) as well as at 26.5°N where continuous observations are available.

4.1. Representation of Water Masses

Any shortcoming in the representation of the AMOC should not be considered in isolation. Instead, it will generally be symptomatic of a variety of model deficiencies (Fox-Kemper et al., 2019) that in turn lead to an unrealistic representation of the water masses in the global ocean that will affect the force balances governing the AMOC (and more generally the global MOC). Of course an AMOC which is either too weak/strong or too shallow/deep can itself be the cause of unrealistic water mass properties; however, there are other contributing factors. Diapycnal mixing is widely accepted as a controlling factor of the MOC; in particular the lower cell of the MOC is a key process affecting water masses but our understanding of its strength and when and where it occurs in the real ocean is still far from complete. Mixing is the subject of past and ongoing observational programs and theoretical and modeling studies (e.g., De Lavergne et al., 2016; Naveira Garabato et al., 2004; MacKinnon et al., 2013; Munk & Wunsch, 1998; Wunsch & Ferrari, 2004). Processes known or suspected to be important for diapycnal mixing (e.g., internal wave/tide breaking) are not yet resolved in global models and are either dealt with using parameterizations or are not represented at all (e.g., De Lavergne et al., 2016; MacKinnon et al., 2017; Nikurashin & Ferrari, 2013). In addition to deficiencies in the representation of diapycnal mixing, models using depth (z) coordinates are subject to undesired numerical mixing of various degrees (e.g., Griffies, Boning, et al., 2000; Lee et al., 2002; Ilicak et al., 2012; Megann, 2018; Gibson et al., 2017) which again affects the ability of models to develop/maintain the correct water mass structure.

A related issue is the difficulty of simulating the flow over sills, such as in the Denmark Strait (e.g., Legg et al., 2009; Roberts & Wood, 1997; Wang et al., 2015; Winton et al., 1998) and generally the flow downsloping topography. Problems with flow over topography lead to a failure of dense waters formed on shelves to reach greater depths. In particular, the difficulty of getting the dense waters from the Denmark Strait to sink to their observed depth suggests that local horizontal grid refinement or the use of a local terrain following coordinate in overflow regions may lead to improvements. Excessively deep mixed layer depths in the Labrador Sea are a signature, in part, of the inability to maintain the supply of dense water from Denmark Strait at the bottom of the Subpolar Gyre. However, some models may be showing a mixed layer deeper than observed, because of temperature and salinity density compensation, and the use of an overly simple delta density criterion for determining the mixed layer depth, that is, depth for which the density difference with the surface exceeds a given threshold (Courtois et al., 2017). Indications are that further increases in resolution improve overflows and water masses in the SPG region, as well as decrease Labrador Sea Water formation rates (e.g., Böning et al., 2016; Li et al., 2019; Garcia-Quintana et al., 2019).

An issue of potentially similar importance is the area where deep convection occurs, which is much larger in models than is believed to be the case in observations (e.g., Feucher et al., 2019). This issue can at least in part be related to resolution and eddy exchange off the west Greenland Current (e.g., Saenko et al., 2017; Chanut et al., 2008). However, that in itself does not seem to be sufficient as the AMOC cell in VIKING005 is still too shallow (and not deeper than other models with poor overflows, Figure 1). It should be noted, however, that the issue of spurious mixing and thus the overflow representation are sensitive to the vertical coordinate of the model (Griffies et al., 2000; Legg et al., 2009). The spurious diapycnal mixing arises in level or terrain-following models because of advective truncation errors and horizontal/isosigma diffusion tensors (Griffies, Pacanowski, & Hallberg, 2000; Marchesiello et al., 2009). Isopycnic models by definition have no numerical diapycnal mixing, and the use of hybrid coordinate systems in HYCOM improves the representation of the overflow water properties and volume transport in the Atlantic (Xu et al., 2010, 2015, 2018; Wang et al., 2015). These simulations also show a more consistent vertical structure of the AMOC transport (Xu

et al., 2012). However, in isopycnal models the diapycnal mixing must be parameterized, and parameterizing subkilometer overflow plume dynamics or interaction with subgrid scale bathymetry remains a challenge (Treguier et al., 2012). Other approaches such as Z-tilde and ALE (Arbitrary Lagrandian Eulerian) coordinates are designed to reduce spurious mixing in the presence of high-frequency vertical isopycnal movements (e.g., linked to internal tides or inertial waves) and to improve the flow over sills (e.g., Petersen et al., 2015; Reckinger et al., 2015; Gibson et al., 2017).

The shortcomings in the representation of the AMOC do not necessarily have their origin in the North Atlantic. For example, one challenge of representation of the Nordic Seas overflow water is to represent the temperature and salinity (hence density) of the overflow source water, which requires an accurate representation of both the heat/freshwater fluxes in the Nordic Seas and the Arctic Ocean, involving complex ocean, atmosphere, and sea/land ice interactions. The representation of the formation of Antarctic bottom water around Antarctica and of Antarctic intermediate water in the ACC is central to simulating a realistic vertical structure of the water masses in the Atlantic. Simulating dense waters formed on the Antarctic shelf to depth suffers from the same problems as Denmark Strait waters in the North Atlantic, and approaches using different coordinate systems are currently being tested. Additionally, the representation of ocean interactions with sea ice/ice shelves which are known to be important for Antarctic deep water formation (Abernathey et al., 2016; Beckmann & Goosse, 2003; Losch, 2008; Asay-Davies et al., 2016) is not yet complete.

Another aspect that has perhaps been somewhat overlooked in high-resolution models, but which could also be important for the vertical AMOC structure, is the choice of the vertical resolution. Most efforts have gone into increasing the horizontal resolution as this is the most obvious change to make to allow us to represent eddies, narrow jet-like currents, and in some instances submesocale features (e.g., Bachman et al., 2017). Increasing horizontal resolution can resolve higher modes with an associated vertical (baroclinic) structure. Often the number of vertical levels is not chosen as to adequately resolve the corresponding baroclinic modal structure (Stewart et al., 2017). It is conceivable that this could affect the vertical AMOC structure as well, and the impact would be dependent on the vertical coordinate used. There are some indications that using a higher number of vertical layers leads to a marginally deeper overturning cell (e.g., Figure 1; compare ORCA0083 simulations run with either 46 or 75 vertical levels). Twin experiments using HYCOM (with 32 and 64 vertical levels) also show that higher vertical resolution leads to slightly weaker diapycnal mixing, and Denmark Strait overflow water extends slightly deeper (Xu et al., 2015).

4.2. Air-Sea Interactions

The atmospheric forcing and the resulting air-sea fluxes are other factors affecting the AMOC. When trying to simulate AMOC events that have occurred in nature, one has to rely on using reanalysis products such as CORE II (e.g., Griffies et al., 2009), DFS (Brodeau et al., 2010), or JRA55-do (Tsujino et al., 2018). For the recent period, where continuous AMOC observations are available, applying observation-derived atmospheric forcing to ocean models has been shown to reproduce the main features of the observed AMOC (e.g., Blaker et al., 2015; Danabasoglu et al., 2014; Xu et al., 2012, 2013). Differences in surface forcing can also partially explain differences in the AMOC, both between models and observations and among different models; regionally these differences can be large (e.g., Long et al., 2017). This will inevitably lead to differences in the evolution of the ocean circulation with implications for the AMOC. Data assimilation does not reduce the differences across models, but rather increases them, because the AMOC variability is very sensitive to the choice of assimilation procedure (Karspeck et al., 2017).

Another issue that applies to reanalyses and to most forced and coupled ocean-atmosphere simulations is that the ocean resolution is higher than that of the atmosphere. This means that air-sea interactions occurring on smaller spatial scales will not be realistic as neither the forcing (nor the atmosphere in the coupled case) can adjust on these small spatial scales. However, observations suggest that the ocean mesoscale does leave an imprint on the atmosphere (e.g., Chelton & Xie, 2010; Frenger et al., 2013).

Of particular importance is the applied restoring timescale toward observed sea surface salinities. This is often (but not always e.g., ECCOv4, Forget et al., 2015) required to keep the models stable in forced configurations because of the uncertainties of the freshwater balance in the reanalysis products. In contrast to the heat forcing, models may exhibit overly sensitive feedbacks and simulate a weaker or drifting AMOC

strength (Griffies et al., 2009). As a result, the applied restoring timescale, typically applied differently by the individual modelling groups, even if the same atmospheric state is used, strongly shapes the AMOC representation (Behrens et al., 2013).

A problem one would face in forced ocean models if we assume that a very high resolution forcing data set were available is that such a forcing would contain features linked to the ocean mesoscale of the real ocean. The mesoscale developing in a model using such a forcing data set would in general be completely decorrelated from the one in the natural ocean, thus introducing a mismatch between forcing and ocean mesoscale. How best to force a high-resolution ocean model with a high-resolution forcing data set is therefore not immediately obvious, but a question will come up as higher-resolution observational data sets increasingly become available. In the coupled case, one can justify a coarser atmospheric resolution by arguing that the Rossby radii are larger in the atmosphere than in the ocean. Coarser atmospheric resolution is also required in order to keep computational cost within feasible limits as at the same resolution an atmospheric model requires shorter integration time steps than the ocean model. However, the use of a coarser atmosphere means that the atmospheric response to ocean mesoscale features may be unrealistically weak, with possible implications for the simulated ocean circulation (including the AMOC). High-resolution coupled simulations suggest qualitative changes in eddy strength from that in uncoupled simulations owing to air-sea feedbacks (Ma et al., 2016; Moreton et al., 2020).

4.3. Computational Cost and Data Volume

An obvious weakness of global (or basin scale) high-resolution models in practical terms resides in their high CPU cost. The latest high-resolution simulations can take many months to complete on HPCs. This means that such models do not allow for the same "playfulness" that one enjoys when using coarse-resolution models (or box models) where one can easily redo/add new simulations, change parameters, scenarios, and so forth. Only a few simulations can realistically be performed at the highest resolutions currently in use, and sensitivity studies to parameter choices are limited. If an unfortunate choice becomes apparent and a run is already quite advanced, it is not always possible to correct this choice and start afresh (as, e.g., the HPC allocation to the associated project may have already been mostly used up). A potential alternative is the use of nested models that allow basin-scale high resolution while maintaining a global embedment through a coarser base model (e.g., North and South Atlantic such as VIKING20X, Rieck et al., 2019). Furthermore, the volume of output to be stored on disk increases proportionally with resolution, and analysis of this output increasingly requires parallel computation. Resolving increasingly smaller and faster varying features also drives the urge to output fields at higher temporal resolution, with many simulations now storing output at daily or 5-daily frequency.

The extreme HPC cost involved in running the latest generation of high-resolution models highlights the importance of international, multi-institute efforts to get a better understanding of the range of behaviors found in such models. Such efforts are the best way to obtain an idea of the range of solutions and sensitivity, for example, DRAKKAR (https://www.drakkarocean.eu), PRIMAVERA (https://www.primavera-h2020.eu), or HighResMIP (Haarsma et al., 2016). In addition, one could also explore the potential of new methodologies to assess uncertainty in the choice of model parameters and how to more efficiently optimize parameter choices (e.g., Williamson et al., 2013, 2017).

A major bottleneck that currently applies to ocean/ocean-atmosphere models is the limit in scalability of the model performance as the number of processors used is increased. When the number of cores is increased to O(10000-20000), performance starts to plateau and increasing the core number even further is detrimental to model performance (e.g., Kiss et al., 2020; Koldunov et al., 2019). Unless there is a step change in processor technology (such as quantum computing, e.g., Arute et al., 2019; Steane, 1998) in the near future, one can assume that the next generation(s) of HPCs will consist of massively parallel machines with millions of cores becoming commonplace. Most, if not all, numerical models are not ready to fully exploit existing massively parallel computers, and if the codes are not adjusted, they will be woefully inadequate to exploit the next generation of HPC. This situation requires major efforts dedicated to rewriting the core of ocean (and atmosphere) models perhaps also with a view to exploit graphical processing units (e.g., Leutwyler et al., 2016; Fuhrer et al., 2018). Such efforts are currently underway. As an example, the Energy Exascale Earth System Model (E3SM) project (e3sm.org), funded by the U.S. Department of Energy, is developing an Earth system model based on highly scalable Earth system components (with MPAS-Ocean being its

variable resolution ocean component). Other examples include IMMERSE (https://immerse-ocean.eu), FESOM (unstructured mesh, Wang et al., 2014; Koldunov et al., 2019), ICON-ESM (e.g., Korn, 2017), MPAS-Ocean (Ringler et al., 2013), and iHESP (https://ihesp.tamu.edu). These efforts are explicitly targeted for highly resolved simulations on the next generation exascale machines.

Closely related to the CPU cost is the huge amount of data produced by these high-resolution simulations. This leads to bottlenecks in the analyses as our ability to analyze new enormous model data sets has not kept pace with our ability to generate them (one single 50- to 100-year simulation with one of the latest high-resolution global models can produce a data volume O(1PB)). Old practices of downloading output to local disks to do the analyses are therefore no longer practical (or realistic). The better practice here is to copy scripts for model analysis to a central data storage with dedicated computing facilities as is the case in, for example, in the PRIMAVERA project (https://www.primavera-h2020.eu). This is an aspect still in need of organization. This requires an international (possibly worldwide) collaborative effort to ensure that the data sets from these simulations have the widest possible reach within the community and beyond to ensure we extract the best science. Sustaining access to these data sets and their analyses may also be critical as teaching sets for novel machine-learning approaches to support data analysis (e.g., Ivezić et al., 2019). Such techniques may represent the best hope for reaching timely conclusions based on the huge data volumes created by future simulations.

5. Discussion and Outlook

In the previous sections we reviewed AMOC features onto which high-resolution ocean models have either shed new light or for which the behavior differs compared with low-resolution models. In this section we provide an overview of the timescales on which the AMOC varies and suggest gaps in our understanding that high-resolution models seem well suited to tackle.

Figure 11 provides an overview of the timescales on which the AMOC can vary and the corresponding amplitude as well as of the underlying processes. Most of the amplitudes are based on models as direct AMOC observations are still sparse in time (mostly at 26°N) and time (starting in 2004). In addition, Figure 11 indicates the importance of AMOC variability for climate on various timescales. On some timescales the importance of the AMOC for climate is well understood (or at least well acknowledged); however, on other timescales it is not yet clear to what extent the AMOC variability feeds back on climate and the importance for climate may be higher or lower than we assume. This is indicated by an envelope of varying width suggesting for which timescales confidence and understanding of the AMOC importance on climate is either high or low. The longest eddy-permitting coupled simulations cover up to about 500 years (Menary et al., 2015). At eddy-rich resolutions the maximum integration length is currently of order 100 years (Griffies et al., 2015; Roberts et al., 2019; Small et al., 2014). Variability estimates on longer timescales rely on either observations (paleo tracers) or coarse-resolution models (e.g., Latif et al., 2019).

In the following we start with the AMOC variability on the shortest (i.e., subdaily to about weekly) timescales, gradually moving to the longer timescales. The largest AMOC variability is found on short timescales and is linked to near-inertial gravity waves (Blaker et al., 2012). With values of up to 50 Sv this variability far exceeds the long-term mean AMOC. However, even though ubiquitous the very large oscillations have a small meridional extent on the order of 100 km and do not signal a speedup/slowdown of the large-scale AMOC. However, models suggest that this variability can propagate equatorward over thousands of kilometers as high amplitude "ripples" in the overturning (Blaker et al., 2012; Figure 8).

The short duration of these AMOC oscillations (from subdaily at midlatitudes to about 7 days in the equatorial region) means that despite their large amplitude they are too short to lead to a significant convergence/divergence of heat. However, we do not yet know whether the presence of such strong high-frequency AMOC variability can affect the long-term mean AMOC. Such changes could, for example, happen via enhanced mixing (the passage of near-inertial waves is associated with a vertical movement of water masses of about 50–100 m/day), or there could be a projection on the AMOC via a Stokes drift associated with the passage of the waves. All of this is of course speculative at this stage, but these high-frequency AMOC features project on both $\psi(z)$ and $\psi(\sigma_2)$ (see section 3.2.1). However, recent work suggests increased mixing linked to equatorially trapped waves in nature as well as in a numerical model (Delorme & Thomas,

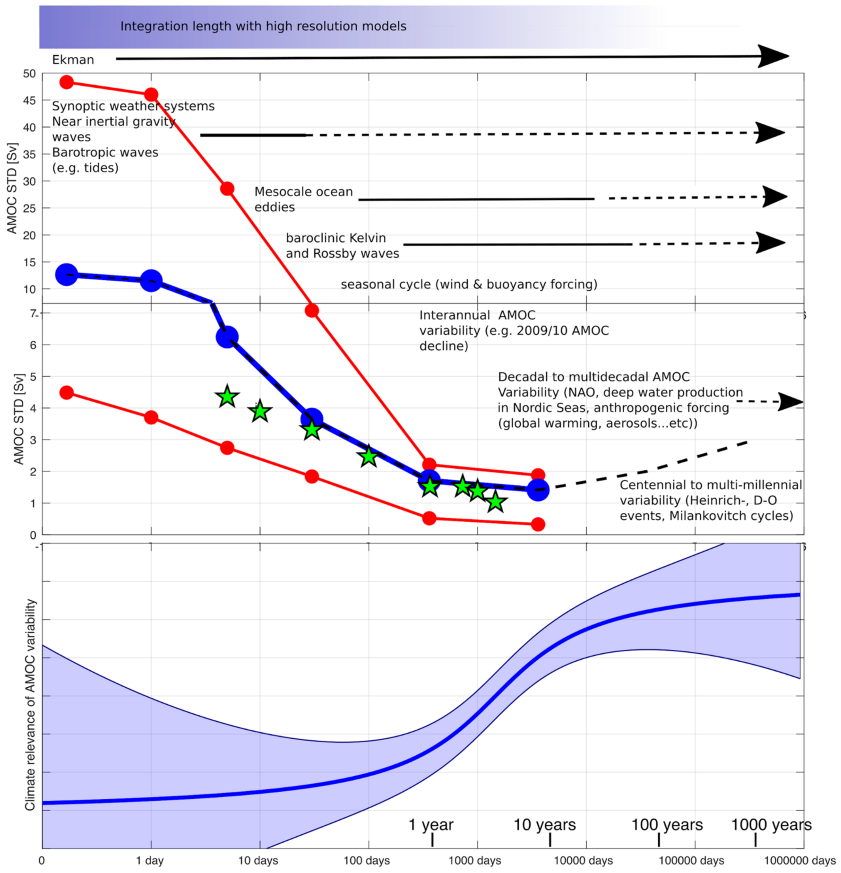

Figure 11. Summary of AMOC variability on timescales ranging from subdaily to millennial. The gradient in the shading of the bar at the top of the figure indicates that all model simulations cover short timescales (dark shading), but only a few high resolution simulations cover 100 years or more (indicated by increasingly light shading for long timescales). Top and middle panels show standard deviations of the AMOC variability in high-resolution models (taken from the values shown in Figure 7). Blue line: average maximum standard deviation between 30°S and 60°N. Red lines: highest and lowest AMOC standard deviation maximum between 30°S and 60°N. Thin black dashed: assumed AMOC standard deviation on multidecadal to millennial timescales. Green stars: AMOC standard deviation obtained from the RAPID AMOC observations at 26.5°N. Arrows with solid lines indicate over what timescales there is high confidence that a given process is affecting the AMOC variability. Dashed lines for the arrows indicate that the importance of a process on a given timescale is uncertain, that is, in particular whether the process in question can affect longer timescales. The bottom panel shows an indicative importance of AMOC variability on different timescales for climate (bold blue line). The spread of the shading indicates for which timescales the uncertainty about the importance of the AMOC is high or low.

2019; Holmes et al., 2016). High-resolution models can help to answer the question whether this enhanced equatorial mixing is due to the large high-frequency AMOC variability seen at the equator.

On weekly to interannual timescales the AMOC variability is much smaller, with a standard deviation of typically up to a few Sv. A variety of processes can influence the AMOC on these timescales: Ekman transports, mesoscale eddies, and internal waves. On these timescales the AMOC variability can be predictable from the surface forcing (Ekman transports), whereas the chaotic/intrinsic variability due to ocean mesoscale eddies, internal waves, and larger-scale instability processes cannot readily be linked to the surface forcing. On monthly to interannual timescales AMOC anomalies can generate significant anomalies in ocean heat content with possible imprint on sea surface temperatures (Alexander-Turner et al., 2018; Bryden et al., 2014; Duchez et al., 2016). The extent to which such variability can impact the atmospheric circulation is far from fully understood. However, there is increasing evidence that this is the case (e.g., Hallam et al., 2019). High-resolution models can help to better understand the relationship between the AMOC and climate/weather timescales (e.g., Hewitt et al., 2017). Increasingly, these models can be run for many decades, sometimes even centuries, thus providing much longer time series for analysis. Such longer

simulations allow us to investigate whether there are systematic links between seasonal to interannual AMOC anomalies and the atmospheric circulation. A particularly important question is whether the AMOC leads the atmosphere in some cases, hence providing the prospect of using the AMOC as a predictor for seasonal weather/climate events (e.g., Duchez et al., 2016; Hallam et al., 2019). The better representation of sharp temperature fronts and the improved position of currents are thought to be a reason for the skill seen in the latest generation of seasonal forecasting systems (e.g., Scaife et al., 2014). However, the underlying processes are far from understood and high-resolution models can provide new insights into the physical processes governing the interactions between AMOC variability and atmosphere on seasonal to decadal timescales.

Decadal timescales have been the subject of many climate studies related to the AMOC and its variability (e.g., Collins & Sinha, 2003; Böning et al., 2006; Wunsch & Heimbach, 2006; Biastoch et al., 2008; Keenlyside et al., 2008; Send et al., 2011; Medhaug et al., 2012; McCarthy et al., 2015). The amplitude of the decadal AMOC variability suggested by models is smaller than on seasonal to interannual timescales but can still be on the order of several Sv (e.g., Latif et al., 2019). The longer duration of such AMOC anomalies means that there is more time for ocean heat content anomalies to build up, thus affecting sea surface temperatures and therefore the atmosphere. Of particular importance on these timescales are links between the Nordic Seas and lower latitudes. Model-based results suggest the Subpolar Gyre, and in particular the Labrador Sea may be a precursor for the AMOC variability further south (e.g., Robson et al., 2014).

As mentioned in section 2 the recent observational results from the OSNAP AMOC observing system and high-resolution simulations may lead us to reassess the respective roles of the Labrador Sea and of the eastern Subpolar Gyre. However, the 21 months of observations are too short to tell whether the respective AMOC variability contributions from the western and eastern Subpolar Gyre will vary over time. This is an important question where high-resolution models can help. As mentioned in section 2, a recent high-resolution coupled simulation shows a dominance (albeit weaker than in OSNAP) of the eastern SPG region for the subpolar AMOC variability. In this particular simulation this dominance remains present throughout the simulation and still applies for decadal timescales. Notably, this result would not change the view that the high-latitude AMOC variability is a likely predictor for the AMOC at lower latitudes.

Another important relationship on decadal timescales is the possible link between the AMOC and the Atlantic multidecadal variability the importance of which for climate is well documented (e.g., Zhang et al., 2019). Currently, it is still not clear whether the Atlantic multidecadal variability develops as a response to changes in the ocean circulation (e.g., McCarthy et al., 2015) or whether it is just a passive response to atmospheric forcing (Clement et al., 2015). In McCarthy et al. (2015) both observations and a model strongly suggest an active role for the ocean circulation in the development of positive or negative AMO phases. However, the sea level-based index used in this study is indicative of an intergyre heat exchange rather than of the AMOC itself. More work is therefore needed to establish the role of the AMOC in the AMO. The latest generation of high-resolution models with their realistic gyre positions and strengths is an ideal tool to investigate these questions.

Multidecadal timescales overlap with the timescales of a long-term AMOC decline in response to global warming. The possibility of changes in the AMOC sensitivity to climate change with increasing model resolution is an area that warrants further work. The existence of a threshold ("tipping point") beyond which the AMOC could undergo abrupt change is still being debated (e.g., Hoffman et al., 2009; Valdes, 2011; Rahmstorf et al., 2015; Liu et al., 2017; Good et al., 2018). Changes in the AMOC pathways and strength of air-sea interactions in high-resolution models could lead us to reassess the sensitivity of the AMOC to anthropogenic climate change.

Simulations for the AMOC on centennial to millennial timescales will remain the domain of coarser-resolution simulations for the foreseeable future. AMOC variability on such timescales (e.g., as presumed to have occurred during Dansgaard-Oeschger events during the last ice age) is thought to have been a major driver for temperature fluctuations of the wider North Atlantic region. Uncertainties are still large, but a significant increase in both available CPU power as well as scalability of models on $O(10^5+)$ cores will be required to consider high-resolution models for studies on centennial to millennial timescales. However, even if such simulations become possible, the sheer cost, not just financially, but also in CO_2 emissions (energy consumption for the top HPC systems can exceed 10 MW), could make them hard to justify. The

future also has to be "smarter"—improved parameterizations and quantification of uncertainty due to parameters and initial conditions (e.g., by making use of machine learning and statistical algorithms), coarsening of output stored on disk, and increased collaborative research and sharing of output. There will come a point when we will have to think carefully about whether what we gain from the next level in resolution is worth the cost.

6. Conclusions

High-resolution ocean models, containing an explicit representation of mesoscale eddies and realistic boundary currents, can be used to address a range of questions regarding the AMOC. Compared to their low-resolution counterparts, high-resolution models simulate AMOC pathways which are in closer agreement with observations. High-resolution ocean models also exhibit AMOC variability which cannot be simulated at low resolutions (e.g., chaotic-intrinsic variability linked to mesoscale ocean eddies) or variability which was previously unknown and which has yet to be observed in nature (e.g., linked to near inertial waves). The implications of this AMOC variability on, for example, mixing and background circulation (and whether it actually exists in nature) are not yet clear, but there is little doubt that future studies will shed more light on it.

With the increasing availability of observational AMOC data from different latitudes (RAPID, OSNAP in the North Atlantic, SAMOC in the South Atlantic), we are entering an era with a unique opportunity to understand AMOC dynamics and to make use of this understanding to improve weather and climate predictions. Although the period covered by continuous AMOC observations remains relatively short (only since 2004), it has been sufficient to prove the existence of large AMOC variability on these timescales. The existence of such variability in models means that they are suited to test if and when the AMOC can be used as a predictor. The main emphasis of many past studies has been dedicated to trying to understand if the AMOC can be predicted (e.g., Pohlmann et al., 2013; Swingedouw et al., 2013). Trying to assess and understand what we can predict, assuming we know the state of the AMOC, is an equally important question for evaluating the practical benefits of AMOC data (e.g., Hallam et al., 2019). The limited period covered by the observational data means that the initial research focus will be on shorter timescales, thus playing into the strengths of high-resolution models as this is where they can now be run almost routinely.

Acknowledgments
We acknowledge constructive comments by Martha Buckley and one anonymous reviewer as well as from Harry Bryden and David Webb. We thank Alain Colin de Verdière for providing the barotropic stream function data. J. H. and A. B. acknowledge funding from the NERC, the NERC RAPID-AMOC project DYNAMOC (NE/M005097/1), and the NERC project ACSIS (NE/N018044/1). This work used the ARCHER U.K. National Supercomputing Service (http://www.archer.ac.uk) and is a contribution to the DRAKKAR project (https://www.drakkarocean.eu). J. S. is partially supported by the International Laboratory for High Resolution Earth System Prediction (iHESP)—a collaboration among the Qingdao National Laboratory for Marine Science and Technology Development Center (QNLM), Texas A&M University (TAMU), and the National Center for Atmospheric Research (NCAR). D. Sein acknowledges the state assignment of FASO Russia (Theme 0149-2019-0015). M. R., D. I., and D. Sein acknowledge PRIMAVERA funding received from the European Commission under Grant Agreement 641727 of the Horizon 2020 research programme, and M. R. and H. H. were supported by the Joint UK BEIS/Defra Met Office Hadley Centre Climate Programme (GA01101). A. K. was funded by the Australian Research Council Linkage Program (LP160100073). L. Thompson acknowledges support from NASA (Grant NNX17AH56G). W. W. was supported by the HiLAT-RASM project of the U.S. Department of Energy's Regional and Global Model Analysis (RGMA) program. The ACCESS-OM2 suite was configured by COSIMA (cosima.org.au) which is funded by the Australian Research Council (Linkage Program LP160100073). It was also supported by the ARC Centre of Excellence for Climate Extremes (Australian Research Council Grant CE170100023) and undertaken using the National Computational Infrastructure (NCI), which is supported by the Australian Government.

References

Abernathey, R. P., Cerovecki, I., Holland, P. R., Newsom, E., Mazloff, M., & Talley, L. D. (2016). Water-mass transformation by sea ice in the upper branch of the Southern Ocean overturning. *Nature Geoscience*, *9*(8), 596.

Aksenov, Y., Ivanov, V. V., Nurser, A. G., Bacon, S., Polyakov, I. V., Coward, A. C., et al. (2011). The Arctic circumpolar boundary current. *Journal of Geophysical Research*, *116*, C09017. https://doi.org/10.1029/2010JC006637

Alexander-Turner, R., Ortega, P., & Robson, J. I. (2018). How Robust Are the Surface Temperature Fingerprints of the Atlantic Overturning Meridional Circulation on Monthly Time Scales? *Geophysical Research Letters*, *45*(8), 3559–3567.

Alford, M. H. (2003). Improved global maps and 54-year history of wind-work on ocean inertial motions. *Geophysical Research Letters*, *30*(8), 1424. https://doi.org/10.1029/2002GL016614

Alford, M. H., MacKinnon, J. A., Simmons, H. L., & Nash, J. D. (2016). Near-inertial internal gravity waves in the ocean. *Annual Review of Marine Science*, *8*, 95–123.

Alkhayuon, H., Ashwin, P., Jackson, L. C., Quinn, C., & Wood, R. A. (2019). Basin bifurcations, oscillatory instability and rate-induced thresholds for AMOC in a global oceanic box model. *Proceedings of the Royal Society of London*, *475*, 20190051. https://doi.org/10.1098/rspa.2019.0051

Amrhein, D. E., Wunsch, C., Marchal, O., & Forget, G. (2018). A global glacial ocean state estimate constrained by upper-ocean temperature proxies. *Journal of Climate*, *31*(19), 8059–8079.

Arbic, B. K., Muller, M., Richman, J. G., Shriver, J. F., Morten, A. J., Scott, R. B., Serazin, G., et al. (2014). Geostrophic turbulence in the frequency-wavenumber domain: Eddy-driven low-frequency variability. *Journal of Physical Oceanography*, *44*(8), 2050–2069.

Arute, F., Arya, K., Babbush, R., Bacon, D., Bardin, J. C., Barends, R., et al. (2019). Quantum supremacy using a programmable superconducting processor. *Nature*, *574*(7779), 505–510.

Asay-Davis, X. S., Cornford, S. L., Durand, G., Galton-Fenzi, B. K., Gladstone, R. M., Gudmundsson, H., et al. (2016). Experimental design for three interrelated marine ice sheet and ocean model intercomparison projects: MISMIP v. 3 (MISMIP+), ISOMIP v. 2 (ISOMIP+) and MISOMIP v. 1 (MISOMIP1). *Geoscientific Model Development*, *9*(7), 2471–2497.

Bachman, S. D., Taylor, J. R., Adams, K. A., & Hosegood, P. J. (2017). Mesoscale and submesoscale effects on mixed layer depth in the Southern Ocean. *Journal of Physical Oceanography*, *47*(9), 2173–2188.

Baehr, J., Hirschi, J., Beismann, J. O., & Marotzke, J. (2004). Monitoring the meridional overturning circulation in the North Atlantic: A model-based array design study. *Journal of Marine Research*, *62*(3), 283–312.

Baringer, M. O., Willis, J., Smeed, D. A., Moat, B., Dong, S., Hobbs, W. R., et al. (2018). Meridional overturning and oceanic heat transport circulation observations in the North Atlantic Ocean [in "State of the Climate in 2017"]. *Bulletin of the American Meteorological Society*, *99*(8), S91–S94.

Beckmann, A., & Goosse, H. (2003). A parameterization of ice shelf–ocean interaction for climate models. *Ocean Modelling*, *5*(2), 157–170.

Behrens, E., Biastoch, A., & Böning, C. W. (2013). Spurious AMOC trends in global ocean sea-ice models related to subarctic freshwater forcing. *Ocean Modelling*, *69*, 39–49.
Bessières, L., Leroux, S., Brankart, J. M., Molines, J. M., Moine, M. P., Bouttier, P. A., et al. (2017). Development of a probabilistic ocean modelling system based on NEMO 3.5: Application at eddying resolution. *Geoscientific Model Development*, *10*(3), 1091–1106.
Biastoch, A., Böning, C. W., Getzlaff, J., Molines, J.-M., & Madec, G. (2008). Causes of interannual-decadal variability in the meridional overturning circulation of the midlatitude North Atlantic Ocean. *Journal of Climate*, *21*, 6599–6615. https://doi.org/10.1175/2008JCLI2404.1
Biastoch, A., Böning, C. W., & Lutjeharms, J. R. E. (2008). Agulhas leakage dynamics affects decadal variability in Atlantic overturning circulation. *Nature*, *456*(7221), 489.
Biastoch, A., Sein, D., Durgadoo, J. V., & Wang, Q. (2018). Simulating the Agulhas system in global ocean models—Nesting vs. multi-resolution unstructured meshes. *Ocean Modelling*, *121*, 117–131. https://doi.org/10.1016/j.ocemod.2017.12.002
Bingham, R. J., & Hughes, C. W. (2008). Determining North Atlantic meridional transport variability from pressure on the western boundary: A model investigation. *Journal of Geophysical Research*, *113*, C09008. https://doi.org/10.1029/2007JC004679
Bingham, R. J., Hughes, C. W., Roussenov, V., & Williams, R. G. (2007). Meridional coherence of the North Atlantic meridional overturning circulation. *Geophysical Research Letters*, *34*, L23606. https://doi.org/10.1029/2007GL031731
Blaker, A. T., Hirschi, J. J., Sinha, B., De Cuevas, B., Alderson, S., Coward, A., & Madec, G. (2012). Large near-inertial oscillations of the Atlantic meridional overturning circulation. *Ocean Modelling*, *42*, 50–56. https://doi.org/10.1016/j.ocemod.2011.11.008
Blaker, A. T., Hirschi, J. J. M., McCarthy, G., Sinha, B., Taws, S., Marsh, R., et al. (2015). Historical analogues of the recent extreme minima observed in the Atlantic meridional overturning circulation at 26°N. *Climate Dynamics*, *44*(1-2), 457–473. https://doi.org/10.1007/s00382-014-2274-6
Bond, G. C., Showers, W., Elliot, M., Evans, M., Lotti, R., Hajdas, I., et al. (1999). The North Atlantic's 1-2 kyr climate rhythm: Relation to Heinrich events, Dansgaard/Oeschger cycles and the Little Ice Age. *Mechanisms of global climate change at millennial time scales*, *112*, 35–58.
Böning, C. W., Behrens, E., Biastoch, A., Getzlaff, K., & Bamber, J. L. (2016). Emerging impact of Greenland meltwater on deepwater formation in the North Atlantic Ocean. *Nature Geoscience*, *9*(7), 523.
Böning, C. W., Bryan, F. O., Holland, W. R., & Doescher, R. (1996). Deep-water formation and meridional overturning in a high-resolution model of the North Atlantic. *Journal of Physical Oceanography*, *26*, 1142–1164.
Böning, C. W., & Herrmann, P. (1994). Annual cycle of poleward heat transport in the ocean: Results from high-resolution modeling of the north and equatorial Atlantic. *Journal of Physical Oceanography*, *24*, 91–107. https://doi.org/10.1175/1520-0485(1994)024<0091:ACOPHT>2.0.CO;2
Böning, C. W., Rhein, M., Dengg, J., & Dorow, C. (2003). Modeling CFC inventories and formation rates of Labrador Sea Water. *Geophysical Research Letters*, *30*(2), 1050. https://doi.org/10.1029/2002GL014855
Böning, C. W., Scheinert, M., Dengg, J., Biastoch, A., & Funk, A. (2006). Decadal variability of subpolar gyre transport and its reverberation in the North Atlantic overturning. *Geophysical Research Letters*, *33*, L21S01. https://doi.org/10.1029/2006GL026906
Bower, A., Lozier, S., & Gary, S. (2011). Export of Labrador Sea water from the subpolar North Atlantic: A Lagrangian perspective. *Deep Sea Research Part II: Topical Studies in Oceanography*, *58*(17-18), 1798–1818. https://doi.org/10.1016/j.dsr2.2010.10.060
Bower, A. S., Lozier, M. S., Gary, S. F., & Böning, C. W. (2009). Interior pathways of the North Atlantic meridional overturning circulation. *Nature*, *459*(7244), 243.
Broecker, W. S. (1987). The biggest chill. *Natural History Magazine*, *97*, 74–82.
Brodeau, L., Barnier, B., Treguier, A. M., Penduff, T., & Gulev, S. (2010). An ERA40-based atmospheric forcing for global ocean circulation models. *Ocean Modelling*, *31*(3-4), 88–104.
Bryden, H. L., & Hall, M. M. (1980). Heat transport by currents across 25°N latitude in the Atlantic Ocean. *Science*, *207*(4433), 884–886.
Bryden, H. L., King, B. A., & McCarthy, G. D. (2011). South Atlantic overturning circulation at 24°S. *Journal of Marine Research*, *69*(1), 38–55.
Bryden, H. L., King, B. A., McCarthy, G. D., & McDonagh, E. L. (2014). Impact of a 30% reduction in Atlantic meridional overturning during 2009-2010. *Ocean Science*, *10* (4), 683–691.
Bryden, H., Longworth, H., & Cunningham, S. (2005). Slowing of the Atlantic meridional overturning circulation at 25°N. *Nature*, *438*, 655–657. https://doi.org/10.1038/nature04385
Buckley, M. W., & Marshall, J. (2016). Observations, inferences, and mechanisms of the Atlantic Meridional Overturning Circulation: A review. *Reviews of Geophysics*, *54*, 5–63. https://doi.org/10.1002/2015RG000493
Cabanes, C., Lee, T., & Lee-Lueng, F. (2008). Mechanisms of interannual variations of the meridional overturning circulation of the North Atlantic Ocean. *Journal of Physical Oceanography*, *38*(2), 467–480.
Caesar, L., Rahmstorf, S., Robinson, A., Feulner, G., & Saba, V. (2018). Observed fingerprint of a weakening Atlantic Ocean overturning circulation. *Nature*, *556*, 191–196. https://doi.org/10.1038/s41586-018-0006-5
Chanut, J., Barnier, B., Large, W., Debreu, L., Penduff, T., Molines, J. M., & Mathiot, P. (2008). Mesoscale eddies in the Labrador Sea and their contribution to convection and restratification. *Journal of Physical Oceanography*, *38*(8), 1617–1643.
Chassignet, E. P., & Marshall, D. P. (2008). Gulf Stream separation in numerical ocean models. *Geophysical Monograph Series*, *177*, 39–61.
Chelton, D. B., Schlax, M. G., Samelson, R. M., & de Szoeke, R. A. (2007). Global observations of large oceanic eddies. *Geophysical Research Letters*, *34*, L15606. https://doi.org/10.1029/2007GL030812
Chelton, D. B., & Xie, S. P. (2010). Coupled ocean-atmosphere interaction at oceanic mesoscales. *Oceanography*, *23*(4), 52–69.
Clement, A., Bellomo, K., Murphy, L. N., Cane, M. A., Mauritsen, T., Radel, G., & Stevens, B. (2015). The Atlantic Multidecadal Oscillation without a role for ocean circulation. *Science*, *350*(6258), 320–324.
Colin de Verdière, A., & Ollitrault, M. (2016). A direct determination of the World Ocean barotropic circulation. *Journal of Physical Oceanography*, *46*(1), 255–273.
Collins, M., Knutti, R., Arblaster, J., Dufresne, J.-L., Fichefet, T., Friedlingstein, P., et al. (2013). Long-term climate change: Projections, commitments and irreversibility. In T. F. Stocker, D. Qin, G.-K. Plattner, M. Tignor, S. K. Allen, J. Boschung, A. Nauels, Y. Xia, V. Bex, & P. M. Midgley (Eds.), *Climate change 2013: The Physical science basis. Contribution of working group I to the fifth assessment report of the intergovernmental panel on climate change* (chap. 12, pp. 1029–1136). Cambridge, United Kingdom and New York, NY, USA: Cambridge University Press.
Collins, M., & Sinha, B. (2003). Predictability of decadal variations in the thermohaline circulation and climate. *Geophysical Research Letters*, *30*(6), 1306. https://doi.org/10.1029/2002GL016504

Courtois, P., Hu, X., Pennelly, C., Spence, P., & Myers, P. G. (2017). Mixed layer depth calculation in deep convection regions in ocean numerical models. *Ocean Modelling*, *120*, 60–78.
Cunningham, S. A., Kanzow, T. O., Rayner, D., Barringer, M. O., Johns, W. E., Marotzke, J., et al. (2007). Temporal variability of the Atlantic Meridional Overturning Circulation at 26.5°N. *Science*, *317*, 935–938.
Danabasoglu, G., Yeager, S. G., Bailey, D., Behrens, E., Bentsen, M., Bi, D., et al. (2014). North Atlantic simulations in coordinated ocean-ice reference experiments phase II (CORE-II). Part I: Mean states. *Ocean Modelling*, *73*, 76–107. https://doi.org/10.1016/j.ocemod.2013.10.005
Danilov, S., Kivman, G., & Schröter, J. (2004). A finite-element ocean model: Principles and evaluation. *Ocean Modelling*, *6*(2), 125–150.
Dansgaard, W., Johnsen, S. J., Clausen, H. B., Dahl-Jensen, D., Gundestrup, N. S., Hammer, C. U., et al. (1993). Evidence for general instability of past climate from a 250-kyr ice-core record. *Nature*, *364*(6434), 218.
De Lavergne, C., Madec, G., Le Sommer, J., Nurser, A. G., & Naveira Garabato, A. C. (2016). On the consumption of Antarctic bottom water in the abyssal ocean. *Journal of Physical Oceanography*, *46*(2), 635–661.
de Vries, P., & Weber, S. L. (2005). The Atlantic freshwater budget as a diagnostic for the existence of a stable shut down of the meridional overturning circulation. *Geophysical Research Letters*, *32*, L09606. https://doi.org/10.1029/2004GL021450
Delorme, B. L., & Thomas, L. N. (2019). Abyssal Mixing through Critical Reflection of Equatorially Trapped Waves off Smooth Topography. *Journal of Physical Oceanography*, *49*, 519–542.
Delworth, T. L., Rosati, A., Anderson, W., Adcroft, A. J., Balaji, V., Benson, R., et al. (2012). Simulated climate and climate change in the GFDL CM2.5 high-resolution coupled climate model. *Journal of Climate*, *25*, 2755–2781. https://doi.org/10.1175/JCLI-D-11-00316.1
Dengg, J., Boning, C., Ernst, U., Redler, R., & Beckmann, A. (1999). Effects of an improved model representation of overflow water on the subpolar North Atlantic. *WOCE Newsletter*, *37*, 10–15.
Dengler, M., Schott, F. A., Eden, C., Brandt, P., Fischer, J., & Zantopp, R. J. (2004). Break-up of the Atlantic deep western boundary current into eddies at 8 S. *Nature*, *432*(7020), 1018.
Deshayes, J., Tréguier, A. M., Barnier, B., Lecointre, A., Sommer, J. L., Molines, J. M., et al. (2013). Oceanic hindcast simulations at high resolution suggest that the Atlantic MOC is bistable. *Geophysical Research Letters*, *40*, 3069–3073. https://doi.org/10.1002/grl.50534
Dijkstra, H. A. (2007). Characterization of the multiple equilibria regime in a global ocean model. *Tellus A: Dynamic Meteorology and Oceanography*, *59*(5), 695–705.
Dong, S., Garzoli, S. L., Baringer, M. O., Meinen, C. S., & Goni, G. J. (2009). Interannual variations in the Atlantic Meridional Overturning Circulation and its relationship with the net northward heat transport in the South Atlantic. *Geophysical Research Letters*, *36*, L20606. https://doi.org/10.1029/2009GL039356
Drijfhout, S., van Oldenborgh, G. J., & Cimatoribus, A. (2012). Is a decline of AMOC causing the warming hole above the North Atlantic in observed and modeled warming patterns. *Journal of Climate*, *25*, 8373–8379. https://doi.org/10.1175/JCLI-D-12-00490.1
Duchez, A., Courtois, P., Harris, E., Josey, S. A., Kanzow, T., Marsh, R., Smeed, D. A., et al. (2016). Potential for seasonal prediction of Atlantic sea surface temperatures using the RAPID array at 26°N. *Climate Dynamics*, *46*(9-10), 3351–3370.
Duchez, A., Frajka-Williams, E., Castro, N., Hirschi, J., & Coward, A. (2014). Seasonal to interannual variability in density around the Canary Islands and their influence on the Atlantic meridional overturning circulation at 26 N. *Journal of Geophysical Research: Oceans*, *119*, 1843–1860. https://doi.org/10.1002/2013JC009416
Dunstone, N., Smith, D., Scaife, A., Hermanson, L., Eade, R., Robinson, N., et al. (2016). Skilful predictions of the winter North Atlantic oscillation one year ahead. *Nature Geoscience*, *9*, 809–814.
Durland, T. S., & Farrar, J. T. (2012). The wavenumber–frequency content of resonantly excited equatorial waves. *Journal of Physical Oceanography*, *42*(11), 1834–1858.
Eden, C., & Willebrand, J. (2001). Mechanism of interannual to decadal variability of the North Atlantic circulation. *Journal of Climate*, *14*(10), 2266–2280.
Elipot, S., Frajka-Williams, E., Hughes, C. W., & Willis, J. K. (2014). The observed North Atlantic Meridional Overturning Circulation: Its meridional coherence and ocean bottom pressure. *Journal of Physical Oceanography*, *44*(2), 517–537.
Farrar, J. T., & Durland, T. S. (2012). Wavenumber-frequency spectra of inertia-gravity and mixed Rossby-gravity waves in the equatorial Pacific Ocean. *Journal of Physical Oceanography*, *42*(11), 1859–1881.
Feucher, C., Garcia-Quintana, Y., Yashayaev, I., Hu, X., & Myers, P. G. (2019). Labrador Sea water formation rate and its impact on the local Meridional Overturning Circulation. *Journal of Geophysical Research: Oceans*, *124*, 5654–5670. https://doi.org/10.1029/2019JC015065
Forget, G., Campin, J.-M., Heimbach, P., Hill, C.N., Ponte, R.M. and Wunsch, C., 2015. ECCO version 4: An integrated framework for non-linear inverse modeling and global ocean state estimation.
Fox, A. D., Haines, K. and de Cuevas, B., 2000. Modelling internal waves with a global ocean model. International WOCE Newsletter, pp.27-30.
Fox-Kemper, B., Adcroft, A., Böning, C. W., Chassignet, E. P., Curchitser, E., Danabasoglu, G., et al. (2019). Challenges and prospects in ocean circulation models. *Frontiers in Marine Science*, *6*, 65. https://doi.org/10.3389/fmars.2019.00065
Frajka-Williams, E. (2015). Estimating the Atlantic overturning at 26°N using satellite altimetry and cable measurements. *Geophysical Research Letters*, *42*, 3458–3464. https://doi.org/10.1002/2015GL063220
Frajka-Williams, E., Ansorge, I. J., Baehr, J., Bryden, H. L., Chidichimo, M. P., Cunningham, S. A., et al. (2019). Atlantic Meridional Overturning Circulation: Observed transports and variability. *Frontiers in Marine Science*, *6*, 260.
Frenger, I., Gruber, N., Knutti, R., & Munnich, M. (2013). Imprint of Southern Ocean eddies on winds, clouds and rainfall. *Nature Geoscience*, *6*(8), 608–612.
Fuhrer, O., Chadha, T., Hoefler, T., Kwasniewski, G., Lapillonne, X., Leutwyler, D., et al. (2018). Near-global climate simulation at 1 km resolution: Establishing a performance baseline on 4888 GPUs with COSMO 5.0. *Geoscientific Model Development*, *11*(4), 1665–1681.
Naveira Garabato, A. C., Polzin, K. L., King, B. A., Heywood, K. J., & Visbeck, M. (2004). Widespread intense turbulent mixing in the Southern Ocean. *Science*, *303*(5655), 210–213.
Garcia-Quintana, Y., Courtois, P., Hu, X., Pennelly, C., Kieke, D., & Myers, P. G. (2019). Sensitivity of Labrador Sea Water formation to changes in model resolution, atmospheric forcing, and freshwater input. *Journal of Geophysical Research: Oceans*, *124*(3), 2126–2152.
Gary, S. F., Lozier, M. S., Böning, C. W., & Biastoch, A. (2011). Deciphering the pathways for the deep limb of the Meridional Overturning Circulation. *Deep Sea Research Part II: Topical Studies in Oceanography*, *58*(17-18), 1781–1797.
Garzoli, S. L., Dong, S., Fine, R., Meinen, C. S., Perez, R. C., Schmid, C., et al. (2015). The fate of the deep western boundary current in the South Atlantic. *Deep Sea Research Part I: Oceanographic Research Papers*, *103*, 125–136.

Gebbie, G. (2014). How much did glacial North Atlantic water shoal? *Paleoceanography*, *29*, 190–209. https://doi.org/10.1002/2013PA002557

Gent, P. R. (2013). Coupled models and climate projections. In G. Siedler, S. M. Griffies, J. Gould, & J. Church (Eds.), *Ocean Circulation and Climate*, (2nd ed., edited bypp. 609–624). Cambridge: Elsevier.

Gent, P. R. (2018). A commentary on the Atlantic meridional overturning circulation stability in climate models. *Ocean Modelling*, *122*, 57–66.

Gibson, A. H., Hogg, A. McC., Kiss, A. E., Shakespeare, C. J., & Adcroft, A. (2017). Attribution of horizontal and vertical contributions to spurious mixing in an Arbitrary Lagrangian–Eulerian ocean model. *Ocean Modelling*, *119*, 45–56.

Good, P., Bamber, J., Halladay, K., Harper, A. B., Jackson, L. C., Kay, G., et al. (2018). Recent progress in understanding climate thresholds: Ice sheets, the Atlantic meridional overturning circulation, tropical forests and responses to ocean acidification. *Progress in Physical Geography: Earth and Environment*, *42*(1), 24–60.

Grégorio, S., Penduff, T., Sérazin, G., Molines, J. M., Barnier, B., & Hirschi, J. (2015). Intrinsic variability of the Atlantic meridional overturning circulation at interannual-to-multidecadal time scales. *Journal of Physical Oceanography*, *45*(7), 1929–1946.

Griffies, S. M., Boning, C., Bryan, F. O., Chassignet, E. P., Gerdes, R., Hasumi, H., et al. (2000). Developments in ocean climate modelling. *Ocean Modelling*, *2*, 461–480.

Griffies, S. M., Böning, C. W., Biastoch, A., Bryan, F., Danabasoglu, G., Chassignet, E., et al. (2009). Coordinated Ocean-ice Reference Experiments (COREs). *Ocean Modelling*, *26*, 1–46. https://doi.org/10.1016/j.ocemod.2008.08.007

Griffies, S. M., Pacanowski, R. C., & Hallberg, R. W. (2000). Spurious diapycnal mixing associated with advection in a z-coordinate ocean model. *Monthly Weather Review*, *128*, 538–564.

Griffies, S. M., & Tziperman, E. (1995). A linear thermohaline oscillator driven by stochastic atmospheric forcing. *Journal of Climate*, *8*, 2440–2453. https://doi.org/10.1175/1520-0442(1995)008<2440:ALTODB>2.0.CO;2

Griffies, S. M., Winton, M., Anderson, W. G., Benson, R., Delworth, T. L., Dufour, C. O., et al. (2015). Impacts on ocean heat from transient mesoscale eddies in a hierarchy of climate models. *Journal of Climate*, *28*, 952–977. https://doi.org/10.1175/JCLI-D-14-00353.1

Grist, J. P., Josey, S. A., & Marsh, R. (2012). Surface estimates of the Atlantic overturning in density space in an eddy-permitting ocean model. *Journal of Geophysical Research: Oceans*, *117*, C6. https://doi.org/10.1029/2011JC007752

Grist, J. P., Josey, S. A., New, A. L., Roberts, M., Koenigk, T., & Iovino, D. (2018). Increasing Atlantic Ocean heat transport in the latest generation coupled ocean-atmosphere models: The role of air-sea interaction. *Journal of Geophysical Research: Oceans*, *123*, 8624–8637. https://doi.org/10.1029/2018JC014387

Haarsma, R. J., Roberts, M. J., Vidale, P. L., Senior, C. A., Bellucci, A., Bao, Q., et al. (2016). High resolution model intercomparison project (HighResMIP v1. 0) for CMIP6. *Geoscientific Model Development*, *9*(1), 4185–4208.

Hall, M. M., & Bryden, H. L. (1980). Direct estimates and mechanisms of ocean heat transport. *Deep Sea Research Part A. Oceanographic Research Papers*, *29*(3), 339–359.

Hallam, S., Marsh, R., Josey, S. A., Hyder, P., Moat, B., & Hirschi, J. J.-M. (2019). Ocean precursors to the extreme Atlantic 2017 hurricane season. *Nature Communications*, *10*(1), 896.

Hawkins, E., Smith, R. S., Allison, L. C., Gregory, J. M., Woollings, T. J., Pohlmann, H., & De Cuevas, B. (2011). Bistability of the Atlantic overturning circulation in a global climate model and links to ocean freshwater transport. *Geophysical Research Letters*, *38*, L10605. https://doi.org/10.1029/2011GL047208

Heinrich, H. (1988). Origin and consequences of cyclic ice rafting in the Northeast Atlantic Ocean during the past 130,000 years. *Quaternary Research*, *29*(2), 142–152.

Heuzé, C. (2017). North Atlantic deep water formation and AMOC in CMIP5 models. *Ocean Science*, *13*, 609–622. https://doi.org/10.5194/os-13-609-2017

Hewitt, H. T., Bell, M. J., Chassignet, E. P., Czaja, A., Ferreira, D., Griffies, S. M., et al. (2017). Will high-resolution global ocean models benefit coupled predictions on short-range to climate timescales? *Ocean Modelling*, *120*, 120–136.

Hewitt, H. T., Roberts, M. J., Hyder, P., Graham, T., Rae, J., Belcher, S. E., et al. (2016). The impact of resolving the Rossby radius at mid-latitudes in the ocean: Results from a high-resolution version of the Met Office GC2 coupled model. *Geoscientific Model Development*, *9*, 3655–3670. https://doi.org/10.5194/gmd-9-3655-2016

Hirschi, J., Baehr, J., Marotzke, J., Stark, J., Cunningham, S., & Beismann, J. O. (2003). A monitoring design for the Atlantic meridional overturning circulation. *Geophysical Research Letters*, *30*(7), 1413. https://doi.org/10.1029/2002GL016776

Hirschi, J. J., Killworth, P. D., & Blundell, J. R. (2007). Subannual, seasonal, and interannual variability of the North Atlantic meridional overturning circulation. *Journal of Physical Oceanography*, *37*(5), 1246–1265. https://doi.org/10.1175/JPO-D-18-0236.1

Hirschi, J. J. M., Blaker, A. T., Sinha, B., Coward, A. C., De Cuevas, B. A., Alderson, S. G., & Madec, G. (2013). Chaotic variability of the meridional overturning circulation on subannual to interannual timescales. *Ocean Science*, *9*, 805–823. https://doi.org/10.5194/os-9-805-2013

Hirschi, J. J. M., Frajka-Williams, E., Blaker, A. T., Sinha, B., Coward, A., Hyder, P., et al. (2019). Loop current variability as trigger of coherent Gulf Stream transport anomalies. *Journal of Physical Oceanography*, *49*(8), 2115–2132. https://doi.org/10.1175/JPO-D-18-0236.1

Hirst, A. C., Jackett, D. R., & McDougall, T. J. (1996). The meridional overturning cells of a world ocean model in neutral density coordinates. *Journal of Physical Oceanography*, *26*(5), 775–791.

Hofmann, M., & Rahmstorf, S. (2009). On the stability of the Atlantic meridional overturning circulation. *Proceedings of the National Academy of Sciences*, *106*(49), 20,584–20,589. https://doi.org/10.1073/pnas.0909146106

Holliday, N. P., Bacon, S., Cunningham, S., Gary, S. F., Karstensen, J., King, B. A., et al. (2018). Subpolar North Atlantic overturning and gyre-scale circulation in the summers of 2014 and 2016. *Journal of Geophysical Research: Oceans*, *123*, 4538–4559. https://doi.org/10.1029/2018JC013841

Holmes, R. M., Moum, J. N., & Thomas, L. N. (2016). Evidence for seafloor-intensified mixing by surface-generated equatorial waves. *Geophysical Research Letters*, *43*, 1202–1210. https://doi.org/10.1002/2015GL066472

Hu, X., Sun, J., Chan, T. O., & Myers, P. G. (2018). Thermodynamic and dynamic ice thickness contributions in the Canadian Arctic Archipelago in NEMO-LIM2 numerical simulations. *The Cryosphere*, *12*(4).

Huck, T., Arzel, O., & Sevellec, F. (2015). Multidecadal variability of the overturning circulation in presence of eddy turbulence. *Journal of Physical Oceanography*, *45*(1), 157–173.

Huisman, S. E., den Toom, M., & Dijkstra, H. A. (2010). An indicator of the multiple equilibria regime of the Atlantic meridional overturning circulation. *Journal of Physical Oceanography*, *40*, 551–567.

Ilicak, M., Adcroft, A. J., Griffies, S. M., & Hallberg, R. W. (2012). Spurious dianeutral mixing and the role of momentum dissipation. *Ocean Modelling*, *45-46*, 37–58. https://doi.org/10.1016/j.ocemod.2011.10.003

Iovino, D., Masina, S., Storto, A., Cipollone, A., & Stepanov, V. N. (2016). A 1/16 eddying simulation of the global NEMO sea-ice-ocean system. *Geoscientific Model Development*, *9*(8), 2665–2684. https://doi.org/10.5194/gmd-9-2665-2016

Ito, K., Kuroda, T., Saito, K., & Wada, A. (2015). Forecasting a large number of tropical cyclone intensities around Japan using a high-resolution atmosphere-ocean coupled model. *Weather and Forecasting*, *30*(3), 793–808.

Ivezić, Ž., Connolly, A. J., VanderPlas, J. T., & Gray, A. (2019). *Statistics, data mining, and machine learning in astronomy: A practical Python guide for the analysis of survey data*. Princeton: Princeton University Press.

Jackson, L. C., Kahana, R., Graham, T., Ringer, M. A., Woollings, T., Mecking, J. V., & Wood, R. A. (2015). Global and European climate impacts of a slowdown of the AMOC in a high resolution GCM. *Climate Dynamics*, *45*, 3299–3316. https://doi.org/10.1007/s00382-015-2540-2

Jackson, L. C., & Wood, R. A. (2018). Hysteresis and resilience of the AMOC in an eddy-permitting GCM. *Geophysical Research Letters*, *45*, 8547–8556. https://doi.org/10.1029/2018GL078104

Jansen, M. F., Nadeau, L. P., & Merlis, T. M. (2018). Transient versus equilibrium response of the ocean's overturning circulation to warming. *Journal of Climate*, *31*(13), 5147–5163.

Johns, W. E., Baringer, M. O., Beal, L. M., Cunningham, S. A., Kanzow, T., Bryden, H. L., et al. (2011). Continuous, array-based estimates of Atlantic Ocean heat transport at 26.5°N. *Journal of Climate*, *24*(10), 2429–2449.

Johnson, H. L., Cessi, P., Marshall, D. P., Schloesser, F., & Spall, M. A. (2019). Recent contributions of theory to our understanding of the Atlantic Meridional Overturning Circulation. *Journal of Geophysical Research: Oceans*, *124*, 5376–5399. https://doi.org/10.1029/2019JC015330

Kanzow, T., Cunningham, S. A., Johns, W. E., Hirschi, J. J.-M., Marotzke, J., Baringer, M. O., et al. (2010). Seasonal variability of the Atlantic meridional overturning circulation at 26.5°N. *Journal of Climate*, *23*, 5678–5698.

Kanzow, T., Cunningham, S. A., Rayner, D., Hirschi, J. J.-M., Johns, W. E., Baringer, M. O., et al. (2007). Observed flow compensation associated with the MOC at 26.5°N in the Atlantic. *Science*, *317*, 938–941.

Kanzow, T., Johnson, H. L., Marshall, D. P., Cunningham, S. A., Hirschi, J. M., Mujahid, A., et al. (2009). Basinwide integrated volume transports in an eddy-filled ocean. *Journal of Physical Oceanography*, *39*(12), 3091–3110.

Kanzow, T., Send, U., Zenk, W., Chave, A.D., & Rhein, M., (2006). Monitoring the integrated deep meridional flow in the tropical North Atlantic: Long-term performance of a geostrophic array. *Deep Sea Research Part I: Oceanographic Research Papers*, *53*(3), 528–546.

Karspeck, A. R., Stammer, D., Köhl, A., Danabasoglu, G., Balmaseda, M., Smith, D. M., et al. (2017). Comparison of the Atlantic meridional overturning circulation between 1960 and 2007 in six ocean reanalysis products. *Climate Dynamics*, *49*(3), 957–982.

Katsman, C. A., Drijfhout, S. S., Dijkstra, H. A., & Spall, M. A. (2018). Sinking of dense North Atlantic waters in a global ocean model: Location and controls. *Journal of Geophysical Research: Oceans*, *123*, 3563–3576. https://doi.org/10.1029/2017JC013329

Keenlyside, N. S., Latif, M., Jungclaus, J., Kornblueh, L., & Roeckner, E. (2008). Advancing decadal-scale climate prediction in the North Atlantic sector. *Nature*, *453*(7191), 84.

Killworth, P. D. (1992). An equivalent-barotropic mode in the Fine Resolution Antarctic Model. *Journal of Physical Oceanography*, *22*(11), 1379–1387.

Kiss, A. E., Hogg, A. McC., Hannah, N., Boeira Dias, F., Brassington, G. B., Chamberlain, M. A., et al. (2020). ACCESS-OM2 v1.0: A global ocean-sea ice model at three resolutions. *Geoscientific Model Development*, *13*(2), 401–442. https://doi.org/10.5194/gmd-13-401-2020https://doi.org/10.5194/gmd-2019-106

Köhl, A. (2005). Anomalies of meridional overturning: Mechanisms in the North Atlantic. *Journal of Physical Oceanography*, *35*(8), 1455–1472.

Koldunov, N. V., Aizinger, V., Rakowsky, N., Scholz, P., Sidorenko, D., Danilov, S., & Jung, T. (2019). Scalability and some optimization of the Finite-volumE Sea ice-Ocean Model, Version 2.0 (FESOM2). *Geoscientific Model Development*, *12*, 3991–4012. https://doi.org/10.5194/gmd-12-3991-2019

Komori, N., Ohfuchi, W., Taguchi, B., Sasaki, H., & Klein, P. (2008). Deep ocean inertia-gravity waves simulated in a high-resolution global coupled atmosphere-ocean GCM. *Geophysical Research Letters*, *35*, L04610. https://doi.org/10.1029/2007GL032807

Korn, P. (2017). Formulation of an unstructured grid model for global ocean dynamics. *Journal of Computational Physics*, *339*, 525–552. https://doi.org/10.1016/j.jcp.2017.03.009

Kuhlbrodt, T., Griesel, A., Montoya, M., Levermann, A., Hofmann, M., & Rahmstorf, S. (2007). On the driving processes of the Atlantic meridional overturning circulation. *Reviews of Geophysics*, *45*, RG2001. https://doi.org/10.1029/2004RG000166

Kuwano-Yoshida, A., Minobe, S., & Xie, S.-P. (2010). Precipitation response to the Gulf Stream in an atmospheric GCM. *Journal of Climate*, *23*(13), 3676–3698.

Latif, M., Park, T., & Park, W. (2019). Decadal Atlantic Meridional Overturning Circulation slowing events in a climate model. *Climate Dynamics*, *53*(1-2), 1111–1124.

Lee, M. M., Coward, A. C., & Nurser, A. G. (2002). Spurious diapycnal mixing of the deep waters in an eddy-permitting global ocean model. *Journal of Physical Oceanography*, *32*(5), 1522–1535.

Lee, T., & Marotzke, J. (1998). Seasonal cycles of meridional overturning and heat transport of the Indian Ocean. *Journal of Physical Oceanography*, *28*, 923–943. https://doi.org/10.1175/1520-0485(1998)028<0923:SCOMOA>2.0.CO;2

Lee, M. M., Nurser, A. G., Coward, A. C., & De Cuevas, B. A. (2009). Effective eddy diffusivities inferred from a point release tracer in an eddy-resolving ocean model. *Journal of Physical Oceanography*, *39*(4), 894–914.

Legg, S., Briegleb, B., Chang, Y., Chassignet, E. P., Danabasoglu, G., Ezer, T., et al. (2009). Improving oceanic overflow representation in climate models: The gravity current entrainment climate process team. *Bulletin of the American Meteorological Society*, *90*(5), 657–670.

Leroux, S., Penduff, T., Bessières, L., Molines, J. M., Brankart, J. M., Sérazin, G., et al. (2018). Intrinsic and atmospherically forced variability of the AMOC: Insights from a large-ensemble ocean hindcast. *Journal of Climate*, *31*(3), 1183–1203.

Leutwyler, D., Fuhrer, O., Lapillonne, X., Lüthi, D., & Schär, C. (2016). Towards European-scale convection-resolving climate simulations with GPUs: A study with COSMO 4.19. *Geoscientific Model Development*, *9*(9), 3393–3412.

Lherminier, P., Mercier, H., Gourcuff, C., Alvarez, M., Bacon, S., & Kermabon, C. (2007). Transports across the 2002 Greenland-Portugal Ovide section and comparison with 1997. *Journal of Geophysical Research*, *112*, C07003. https://doi.org/10.1029/2006JC003716

Li, F., Lozier, M. S., Danabasoglu, G., Holliday, N. P., Kwon, Y. O., Romanou, A., et al. (2019). Local and downstream relationships between Labrador Sea Water volume and North Atlantic meridional overturning circulation variability. *Journal of Climate*, *32*(13), 3883–3898.

Liu, W., Xie, S. P., Liu, Z., & Zhu, J. (2017). Overlooked possibility of a collapsed Atlantic Meridional Overturning Circulation in warming climate. *Science Advances*, *3*(1), e1601666.

Long, C., Fujiwara, M., Davis, S. M., Mitchell, D. M., & Wright, C. J. (2017). Climatology and interannual variability of dynamic variables in multiple reanalyses evaluated by the SPARC Reanalysis Intercomparison Project (S-RIP). *Atmospheric Chemistry and Physics*, *17*(23).

Longworth, H., Marotzke, J., & Stocker, T. F. (2005). Ocean gyres and abrupt change in the thermohaline circulation: A conceptual analysis. *Journal of Climate*, *18*(13), 2403–2416.
Losch, M. (2008). Modeling ice shelf cavities in az coordinate ocean general circulation model. *Journal of Geophysical Research*, *113*, C08043. https://doi.org/10.1029/2007JC004368
Lozier, M. S. (1997). Evidence for large-scale eddy-driven gyres in the North Atlantic. *Science*, *277*(5324), 361–364. https://doi.org/10.1126/science.277.5324.361
Lozier, M. S. (1999). The impact of mid-depth recirculations on the distribution of tracers in the North Atlantic. *Geophysical Research Letters*, *26*(2), 219–222.
Lozier, M. S. (2010). Deconstructing the conveyor belt. *Science*, *328*, 1507–1511.
Lozier, M. S., Gary, S. F., & Bower, A. S. (2013). Simulated pathways of the overflow waters in the North Atlantic: Subpolar to subtropical export. *Deep Sea Research Part II: Topical Studies in Oceanography*, *85*, 147–153.
Lozier, M. S., Li, F., Bacon, S., Bahr, F., Bower, A. S., Cunningham, S. A., et al. (2019). A sea change in our view of overturning in the subpolar North Atlantic. *Science*, *363*(6426), 516–521.
Lozier, S. M., Bacon, S., Bower, A. S., Cunningham, S. A., Femke de Jong, M., De Steur, L., et al. (2017). Overturning in the Subpolar North Atlantic Program: A new international ocean observing system. *Bulletin of the American Meteorological Society*, *98*(4), 737–752.
Lumpkin, R., & Speer, K. (2007). Global ocean meridional overturning. *Journal of Physical Oceanography*, *37*(10), 2550–2562. https://doi.org/10.1175/JPO3130.1
Lutjeharms, J. R. E., & Webb, D. J. (1995). Modelling the Agulhas current system with FRAM (fine resolution Antarctic model). *Deep Sea Research Part I: Oceanographic Research Papers*, *42*(4), 523–551.
Lutjeharms, J. R. E., Webb, D. J., de Cuevas, B. A., & Thompson, S. R. (1995). Large-scale modelling of the South-East Atlantic upwelling system. *South African Journal of Marine Science*, *16*(1), 205–225. https://doi.org/10.2989/025776195784156665
Lynch-Stieglitz, J. (2017). The Atlantic meridional overturning circulation and abrupt climate change. *Annual Review of Marine Science*, *9*, 83–104.
Ma, X., Jing, Z., Chang, P., Liu, X., Montuoro, R., Small, R. J., et al. (2016). Western boundary currents regulated by interaction between ocean eddies and the atmosphere. *Nature*, *535*(7613), 533.
MacKinnon, J. A., Laurent, L. S., & Naveira Garabato, A. C. (2013). Diapycnal mixing processes in the ocean interior, in Ocean Circulation and Climate. In G. Siedler, S. M. Griffies, J. Gould, & J. Church (Eds.), *A 21st century perspective*, edited by, (2nd ed.pp. 159–183). Amsterdam: Elsevier.
MacKinnon, J. A., Zhao, Z., Whalen, C. B., Waterhouse, A. F., Trossman, D. S., Sun, O. M., et al. (2017). Climate process team on internal-wave driven ocean mixing. *Bulletin of the American Meteorological Society*, *98*(11), 2429–2454. https://doi.org/10.1175/BAMS-D-16-0030.1
Maltrud, M. E., Smith, R. D., Semtner, A. J., & Malone, R. C. (1998). Global eddy-resolving ocean simulations driven by 1985–1995 atmospheric winds. *Journal of Geophysical Research*, *103*, 30,825–30,853.
Manabe, S., & Stouffer, R. J. (1988). Two stable equilibria of a coupled ocean-atmosphere model. *Journal of Climate*, *1*, 841–866.
Marchesiello, P. L., Debreu, L., & Couvelard, X. (2009). Spurious diapycnal mixing in terrain-following coordinate models: The problem and a solution. *Ocean Modelling*, *26*, 156–169.
Marotzke, J., Welander, P., & Willebrand, J. (1988). Instability and multiple steady states in a meridional-plane model of the thermohaline circulation. *Tellus A: Dynamic Meteorology and Oceanography*, *40*(2), 162–172.
Marsh, R., de Cuevas, B. A., Coward, A. C., Jacquin, J., Hirschi, J. J.-M., Aksenov, Y., et al. (2009). Recent changes in the North Atlantic circulation simulated with eddy-permitting and eddy-resolving ocean models. *Ocean Modelling*, *28*(4), 226–239.
Marzocchi, A., Hirschi, J. J. M., Holliday, N. P., Cunningham, S. A., Blaker, A. T., & Coward, A. C. (2015). The North Atlantic subpolar circulation in an eddy-resolving global ocean model. *Journal of Marine Systems*, *142*, 126–143. https://doi.org/10.1016/j.jmarsys.2014.10.007
Mashayek, A., Ferrari, R., Nikurashin, M., & Peltier, W. R. (2015). Influence of enhanced abyssal diapycnal mixing on stratification and the ocean overturning circulation. *Journal of Physical Oceanography*, *45*(10), 2580–2597.
McCarthy, G., Frajka-Williams, E., Johns, W. E., Baringer, M. O., Meinen, C. S., Bryden, H. L., et al. (2012). Observed interannual variability of the Atlantic meridional overturning circulation at 26.5 N. *Geophysical Research Letters*, *39*(19).
McCarthy, G. D., Smeed, D. A., Johns, W. E., Frajka-Williams, E., Moat, B. I., Rayner, D., et al. (2015). Measuring the Atlantic meridional overturning circulation at 26°N. *Progress in Oceanography*, *130*, 91–111.
McClean, J. L., Poulain, P.-M.,Pelton, J. W., & Maltrud, M. E. (2002). Eulerian and Lagrangian statistics from surface drifters and a high-resolution POP simulation in the North Atlantic. *Journal of Physical Oceanography*, *32*, 2472–2491. https://doi.org/10.1175/1520-0485-32.9.2472
McDonagh, E. L., & King, B. A. (2005). Oceanic fluxes in the South Atlantic. *Journal of Physical Oceanography*, *35*(1), 109–122.
Mecking, J. V., Drijfhout, S. S., Jackson, L. C., & Andrews, M. B. (2017). The effect of model bias on Atlantic freshwater transport and implications for AMOC bi-stability. *Tellus A: Dynamic Meteorology and Oceanography*, *69*(1), 1299910.
Mecking, J. V., Drijfhout, S. S., Jackson, L. C., & Graham, T. (2016). Stable AMOC off state in an eddy-permitting coupled climate model. *Climate Dynamics*, *47*(7-8), 2455–2470.
Medhaug, I., Langehaug, H. R., Eldevik, T., Furevik, T., & Bentsen, M. (2012). Mechanisms for decadal scale variability in a simulated Atlantic meridional overturning circulation. *Climate Dynamics*, *39*(1-2), 77–93.
Megann, A. (2018). Estimating the numerical diapycnal mixing in an eddy-permitting ocean model. *Ocean Modelling*, *121*, 19–33.
Menary, M. B., Hodson, D. L., Robson, J. I., Sutton, R. T., & Wood, R. A. (2015). A mechanism of internal decadal Atlantic Ocean variability in a high-resolution coupled climate model. *Journal of Climate*, *28*(19), 7764–7785.
Merz, A. (1925). Die Deutsche Atlantische Expedition auf dem Vermessungs und Forschungsschiff Meteor. Vorbericht, Sitzungsberichten der Physikalish-Mathematischen Klasse der Preussischen Akademie der Wissenschaften, *No. XXXI*.
Mercier, H., Lherminier, P., Sarafanov, A., Gaillard, F., Daniault, N., Desbruyères, D., et al. (2015). Variability of the meridional overturning circulation at the Greenland–Portugal OVIDE section from 1993 to 2010. *Progress in Oceanography*, *132*, 250–261.
Minobe, S., Kuwano-Yoshida, A., Komori, N., Xie, S. P., & Small, R. J. (2008). Influence of the Gulf Stream on the troposphere. *Nature*, *452*(7184), 206.
Minobe, S., Miyashita, M., Kuwano-Yoshida, A., Tokinaga, H., & Xie, S. P. (2010). Atmospheric response to the Gulf Stream: Seasonal variations. *Journal of Climate*, *23*(13), 3699–3719.
Moat, B. I., Josey, S. A., Sinha, B., Blaker, A. T., Smeed, D. A., McCarthy, G., et al. (2016). Major variations in subtropical North Atlantic heat transport at short (5 day) timescales and their causes. *Journal of Geophysical Research: Oceans*, *121*, 3237–3249. https://doi.org/10.1002/2016JC011660

Moreton, S., Ferreira, D., Roberts, M., & Hewitt, H. (2020). Evaluating surface eddy properties in coupled climate simulations with 'eddy-present' and 'eddy-rich' ocean resolution. *Ocean Modelling*, 101567.

Moffa-Sánchez, P., Moreno-Chamarro, E., Reynolds, D. J., Ortega, P., Cunningham, L., Swingedouw, D., et al. (2019). Variability in the northern North Atlantic and Arctic oceans across the last two millennia: A review. *Paleoceanography and Paleoclimatology*, *34*(8), 1399–1436. https://doi.org/10.1029/2018PA003508

Müller, V., Kieke, D., Myers, P. G., Pennelly, C., & Mertens, C. (2017). Temperature flux carried by individual eddies across 47°N in the Atlantic Ocean. *Journal of Geophysical Research: Oceans*, *122*, 2441–2464. https://doi.org/10.1002/2016JC012175

Munk, W., & Wunsch, C. (1998). Abyssal recipes II: Energetics of tidal and wind mixing. *Deep Sea Research Part I: Oceanographic Research Papers*, *45*(12), 1977–2010.

Murakami, H., Vecchi, G. A., Underwood, S., Delworth, T. L., Wittenberg, A. T., Anderson, W. G., et al. (2015). Simulation and prediction of category 4 and 5 hurricanes in the high-resolution GFDL HiFLOR coupled climate model. *Journal of Climate*, *28*(23), 9058–9079.

Nikurashin, M., & Ferrari, R. (2013). Overturning circulation driven by breaking internal waves in the deep ocean. *Geophysical Research Letters*, *40*, 3133–3137. https://doi.org/10.1002/grl.50542

Nurser, A. G., & Lee, M. M. (2004). Isopycnal averaging at constant height. Part I: The formulation and a case study. *Journal of Physical Oceanography*, *34*(12), 2721–2739.

Paiva, A. M., Hargrove, J. T., Chassignet, E. P., & Bleck, R. (1999). Turbulent behavior of a fine mesh (1/12°) numerical simulation of the North Atlantic. *Journal of Marine Systems*, *21*, 307–320.

Penduff, T., Barnier, B., Terray, L., Bessières, L., Sérazin, G., Gregorio, S., et al. (2014). Ensembles of eddying ocean simulations for climate. *CLIVAR Exchanges*, Special Issue on High Resolution Ocean Climate Modelling, 19.

Penduff, T., Juza, M., Brodeau, L., Smith, G. C., Barnier, B., Molines, J.-M., et al. (2010). Impact of global ocean model resolution on sea-level variability with emphasis on interannual time scales. *Ocean Science*, *6*, 269–284.

Perez, F. F., Fontela, M., García-Ibáñez, M. I., Mercier, H., Velo, A., Lherminier, P., et al. (2018). Meridional overturning circulation conveys fast acidification to the deep Atlantic Ocean. *Nature*, *554*(7693), 515–518. https://doi.org/10.1038/nature25493

Perez, R. C., Baringer, M. O., Dong, S., Garzoli, S. L., Goes, M., Goni, G. J., et al. (2015). Measuring the Atlantic meridional overturning circulation. *Marine Technology Society Journal*, *49*(2), 167–177. https://doi.org/10.4031/MTSJ.49.2.14

Perez, R. C., Garzoli, S. L., Meinen, C. S., & Matano, R. P. (2011). Geostrophic velocity measurement techniques for the meridional overturning circulation and meridional heat transport in the South Atlantic. *Journal of Atmospheric and Oceanic Technology*, *28*, 1504–1521.

Pérez, F., Mercier, H., Vázquez-Rodríguez, M., Lherminier, P., Velo, A., Pardo, P. C., Rosón, G., & Ríos, A. F. (2013). Atlantic Ocean CO_2 uptake reduced by weakening of the meridional overturning circulation. *Nature Geoscience*, *6*, 146–152. https://doi.org/10.1038/ngeo1680

Petersen, M. R., Jacobsen, D. W., Ringler, T. D., Hecht, M. W., & Maltrud, M. E. (2015). Evaluation of the arbitrary Lagrangian–Eulerian vertical coordinate method in the MPAS-Ocean model. *Ocean Modelling*, *86*, 93–113.

Pickart, R. S., & Spall, M. A. (2007). Impact of Labrador Sea convection on the North Atlantic meridional overturning circulation. *Journal of Physical Oceanography*, *37*(9), 2207–2227.

Pohlmann, H., Smith, D. M., Balmaseda, M. A., Keenlyside, N. S., Masina, S., Matei, D., et al. (2013). Predictability of the mid-latitude Atlantic meridional overturning circulation in a multi-model system. *Climate Dynamics*, *41*(3-4), 775–785.

Rahmstorf, S. (1996). On the freshwater forcing and transport of the Atlantic thermohaline circulation. *Climate Dynamics*, *12*(12), 799–811.

Rahmstorf, S., Box, J. E., Feulner, G., Mann, M. E., Robinson, A., Rutherford, S., & Schaffernicht, E. J. (2015). Exceptional twentieth-century slowdown in Atlantic Ocean overturning circulation. *Nature Climate Change*, *5*(5), 475. https://doi.org/10.1038/NCLIMATE2554

Rahmstorf, S., & Ganopolski, A. (1999). Long-term global warming scenarios computed with an efficient coupled climate model. *Climatic Change*, *43*, 353–367.

Rayner, D., Hirschi, J. J. M., Kanzow, T., Johns, W. E., Wright, P. G., Frajka-Williams, E., et al. (2011). Monitoring the Atlantic meridional overturning circulation. *Deep-Sea Research Part II: Topical Studies in Oceanography*, *58*(17-18), 1744–1753. https://doi.org/10.1016/j.dsr2.2010.10.056

Reckinger, S. M., Petersen, M. R., & Reckinger, S. J. (2015). A study of overflow simulations using MPAS-Ocean: Vertical grids, resolution, and viscosity. *Ocean Modelling*, *96*, 291–313.

Reintges, A., Martin, T., Latif, M., & Keenlyside, N. S. (2017). Uncertainty in twenty-first century projections of the Atlantic Meridional Overturning Circulation in CMIP3 and CMIP5 models. *Climate Dynamics*, *49*, 1495–1511. https://doi.org/10.1007/s00382-016-3180-x

Richards, K. J., Maximenko, N. A., Bryan, F. O., & Sasaki, H. (2006). Zonal jets in the Pacific Ocean. *Geophysical Research Letters*, *33*, L03605. https://doi.org/10.1029/2005GL024645

Rieck, J. K., Böning, C. W., & Getzlaff, K. (2019). The nature of eddy kinetic energy in the Labrador Sea: Different types of mesoscale eddies, their temporal variability and impact on deep convection. *Journal of Physical Oceanography*, *49*(8), 2075–2094. https://doi.org/10.1175/JPO-D-18-0243.1

Ringler, T., Petersen, M., Higdon, R. L., Jacobsen, D., Jones, P. W., & Maltrud, M. (2013). A multi-resolution approach to global ocean modeling. *Ocean Modelling*, *69*, 211–232.

Roberts, M. J., Baker, A., Blockley, E. W., Calvert, D., Coward, A., Hewitt, H. T., et al. (2019). Description of the resolution hierarchy of the global coupled HadGEM3-GC3.1 model as used in CMIP6 HighResMIP experiments. *Geoscientific Model Development Discussion*. https://doi.org/10.5194/gmd-2019-148, in review

Roberts, M. J., Hewitt, H. T., Hyder, P., Ferreira, D., Josey, S. A., Mizielinski, M., & Shelly, A. (2016). Impact of ocean resolution on coupled air-sea fluxes and large-scale climate. *Geophysical Research Letters*, *43*, 10–430. https://doi.org/10.1002/2016GL070559

Roberts, M. J., Vidale, P. L., Senior, C., Hewitt, H. T., Bates, C., Berthou, S., et al. (2018). The benefits of global high-resolution for climate simulation: Process-understanding and the enabling of stakeholder decisions at the regional scale. *Bulletin of the American Meteorological Society*, *99*(11), 2341–2359. https://doi.org/10.1175/BAMS-D-15-00320.1

Roberts, M. J., & Wood, R. A. (1997). Topographic sensitivity studies with a Bryan-Cox-type ocean model. *Journal of Physical Oceanography*, *27*, 823–836. https://doi.org/10.1175/1520-0485(1997)027<0823:TSSWAB>2.0.CO;2

Robson, J., Hodson, D., Hawkins, E., & Sutton, R. (2014). Atlantic overturning in decline? *Nature Geoscience*, *7*(1), 2.

Saenko, O. A., Yang, D., & Myers, P. G. (2017). Response of the North Atlantic dynamic sea level and circulation to Greenland meltwater and climate change in an eddy-permitting ocean model. *Climate Dynamics*, *49*(7-8), 2895–2910. Saunders, P. M., Coward, A. C., & de Cuevas, B. A. (1999). The circulation of the Pacific Ocean seen in a Global Ocean Model (OCCAM). *Journal of Geophysical Research*, *104*, 18,281–18,299.

Scaife, A. A.,Arribas, A., Blockley, E., Brookshaw, A., Clark, R. T., Dunstone, N., et al. (2014). Skillful long-range prediction of European and North American winters. *Geophysical Research Letters*, *41*, 2514–2519. https://doi.org/10.1002/2014GL059637

Sinha, B., Smeed, D. A., McCarthy, G., Moat, B. I., Josey, S. A., Hirschi, J.J.-M., et al. (2018). The accuracy of estimates of the overturning circulation from basin-wide mooring arrays. *Progress in Oceanography*, *160*, 101–123. https://doi.org/10.1016/j.pocean.2017.12.001

Sein, D. V., Danilov, S., Biastoch, A., Durgadoo, J. V., Sidorenko, D., Harig, S., & Wang, Q. (2016). Designing variable ocean model resolution based on the observed ocean variability. *Journal of Advances in Modeling Earth Systems*, *8*, 904–916. https://doi.org/10.1002/2016MS000650

Sein, D. V., Koldunov, N. V., Danilov, S., Sidorenko, D., Wekerle, C., Cabos, W., et al. (2018). The relative influence of atmospheric and oceanic model resolution on the circulation of the North Atlantic Ocean in a coupled climate model. *Journal of Advances in Modeling Earth Systems*, *10*, 2026–2041. https://doi.org/10.1029/2018MS001327

Sein, D. V., Koldunov, N. V., Danilov, S., Wang, Q., Sidorenko, D., Fast, I., et al. (2017). Ocean modeling on a mesh with resolution following the local Rossby radius. *Journal of Advances in Modeling Earth Systems*, *9*, 2601–2614. https://doi.org/10.1002/2017MS001099

Semtner, A. J. Jr., & Chervin, R. M. (1988). A simulation of the global ocean circulation with resolved eddies. *Journal of Geophysical Research*, *93*(C12), 15,502–15,522.

Semtner, A. J. Jr., & Mintz, Y. (1977). Numerical simulation of the Gulf Stream and mid-ocean eddies. *Journal of Physical Oceanography*, *7*(2), 208–230.

Send, U., Lankhorst, M., & Kanzow, T. (2011). Observation of decadal change in the Atlantic meridional overturning circulation using 10 years of continuous transport data. *Geophysical Research Letters*, *38*, L24606. https://doi.org/10.1029/2011GL049801

Sérazin, G., Penduff, T., Barnier, B., Molines, J. M., Arbic, B. K., Müller, M., & Terray, L. (2018). Inverse cascades of kinetic energy as a source of intrinsic variability: A global OGCM study. *Journal of Physical Oceanography*, *48*(6), 1385–1408.

Sévellec, F., Hirschi, J. J. M., & Blaker, A. T. (2013). On the Near-Inertial Resonance of the Atlantic Meridional Overturning Circulation. *Journal of Physical Oceanography*, *43*(12), 2661–2672.

Siqueira, L., & Kirtman, B. P. (2016). Atlantic near-term climate variability and the role of a resolved Gulf Stream. *Geophysical Research Letters*, *43*, 3964–3972. https://doi.org/10.1002/2016GL068694

Sévellec, F., & Fedorov, A. V. (2013). The leading, interdecadal eigenmode of the Atlantic meridional overturning circulation in a realistic ocean model. *Journal of Climate*, *26*(7), 2160–2183.

Small, R. J., Bacmeister, J., Bailey, D., Baker, A., Bishop, S., Bryan, F., et al. (2014). A new synoptic scale resolving global climate simulation using the Community Earth System Model. *Journal of Advances in Modeling Earth Systems*, *6*, 1065–1094. https://doi.org/10.1002/2014MS000363

Small, R. J., Msadek, R., Kwon, Y. O., Booth, J. F., & Zarzycki, C. (2018). Atmosphere surface storm track response to resolved ocean mesoscale in two sets of global climate model experiments. *Climate Dynamics*, *52*(3-4), 2067–2089.

Smeed, D. A., Josey, S. A., Beaulieu, C., Johns, W. E., Moat, B. I., Frajka-Williams, E., et al. (2018). The North Atlantic Ocean is in a state of reduced overturning. *Geophysical Research Letters*, *45*, 1527–1533. https://doi.org/10.1002/2017GL076350

Smeed, D. A., McCarthy, G. D., Cunningham, S. A., Frajka-Williams, E., Rayner, D., Johns, W. E., et al. (2014). Observed decline of the Atlantic meridional overturning circulation 2004–2012. *Ocean Science*, *10*, 29–38. https://doi.org/10.5194/os-10-29-2014

Smith, R. D., Maltrud, M. E., Bryan, F. O., & Hecht, M. W. (2000). Numerical simulation of the North Atlantic Ocean at 1/10°. *Journal of Physical Oceanography*, *30*, 1532–1561.

Spence, P., Saenko, O. A., Sijp, W., & England, M. H. (2013). North Atlantic climate response to Lake Agassiz drainage at coarse and ocean eddy-permitting resolutions. *Journal of Climate*, *26*(8), 2651–2667. https://doi.org/10.1175/JCLI-D-11-00683.1

Steane, A. (1998). Quantum computing. *Reports on Progress in Physics*, *61*(2), 117.

Stepanov, V. N., Iovino, D., Masina, S., Storto, A., & Cipollone, A. (2016). Observed and simulated variability of the Atlantic Meridional Overturning Circulation at 41° N. *Journal of Marine Systems*, *164*, 42–52.

Stevens, D. P. (1991). The open boundary condition in the United Kingdom fine-resolution Antarctic model. *Journal of Physical Oceanography*, *21*(9), 1494–1499.

Stewart, K. D., Hogg, A. McC., Griffies, S. M., Heerdegen, A. P., Ward, M. L., Spence, P., & England, M. H. (2017). Vertical resolution of baroclinic modes in global ocean models. *Ocean Modelling*, *113*, 50–65. https://doi.org/10.1016/j.ocemod.2017.03.012

Stocker, T. F. (2013). The ocean as a component of the climate system. In G. Siedler, S. M. Griffies, J. Gould, & J. Church (Eds.), *Ocean Circulation and Climate*, (2nd ed., edited bypp. 3–30). Amsterdam: Elsevier.

Stocker, T. F., Qin, D., Plattner, G.-K., Tignor, M., Allen, S. K., Boschung, J., et al. (Eds.) (2014). Climate Change 2013: The Physical Science Basis (1535 pp.). Cambridge University Press.

Stommel, H. (1961). Thermohaline convection with two stable regimes of flow. *Tellus*, *13*(2), 224–230.

Swingedouw, D., Mignot, J., Labetoulle, S., Guilyardi, E., & Madec, G. (2013). Initialisation and predictability of the AMOC over the last 50 years in a climate model. *Climate Dynamics*, *40*(9-10), 2381–2399.

Talandier, C., Deshayes, J., Treguier, A. M., Capet, X., Benshila, R., Debreu, L., et al. (2014). Improvements of simulated Western North Atlantic current system and impacts on the AMOC. *Ocean Modelling*, *76*, 1–19.

Tatebe, H., Ogura, T., Nitta, T., Komuro, Y., Ogochi, K., Takemura, T., et al. (2019). Description and basic evaluation of simulated mean state, internal variability, and climate sensitivity in MIROC6. *Geoscientific Model Development*, *12*(7), 2727–2765. https://doi.org/10.5194/gmd-12-2727-2019

The FRAM GROUP (1991). An eddy-resolving model of the Southern Ocean. *Eos, Transactions of the American Geophysical Union*, *72*(169), 174–175.

Thomas, M. D., & Fedorov, A. V. (2019). Mechanisms and impacts of a partial AMOC recovery under enhanced freshwater forcing. *Geophysical Research Letters*, *46*, 3308–3316. https://doi.org/10.1029/2018GL080442

Thornalley, D. J. R., Oppo, D. W., Ortega, P., Robson, J. I., Brierley, C. M., Davis, R., et al. (2018). Anomalously weak Labrador Sea convection and Atlantic overturning during the past 150 years. *Nature*, *556*(7700), 227–230. https://doi.org/10.1038/s41586-018-0007-4

Treguier, A. M., Claire, G., Lherminier, P., Mercier, H., Barnier, B., Madec, G., et al. (2006). Internal and forced variability along a section between Greenland and Portugal in the CLIPPER Atlantic model. *Ocean Dynamics*, *56*, 568–580. https://doi.org/10.1007/s10236-006-0069-y

Treguier, A. M., Ferron, B., & Dussin, R. (2012). Buoyancy driven currents in eddying ocean models. In E. Chassignet, & J. Verron (Eds.), *Buoyancy driven flows* (chap. 7, pp. 281–311). Cambridge: Cambridge University Press.

Treguier, A.-M., Reynaud, T., Pichevin, T., Barnier, B., Molines, J. M., De Miranda, A. P., et al. (1999). The CLIPPER project: High resolution modeling of the Atlantic. *International WOCE Newsletter*, *36*, 3–5.

Treguier, A. M., Theetten, S., Chassignet, E., Penduff, T., Smith, R., Talley, L., et al. (2005). The North Atlantic subpolar gyre in four high resolution models. *Journal of Physical Oceanography*, *35*, 757–774.
Tsujino, H., Urakawa, S., Nakano, H., Small, R. J., Kim, W. M., Yeager, S. G., et al. (2018). JRA-55 based surface dataset for driving ocean-sea-ice models (JRA55-do). *Ocean Modelling*, *130*, 79–139. https://doi.org/10.1016/j.ocemod.2018.07.002
Valdes, P. (2011). Built for stability. *Nature Geoscience*, *4*(7), 414.
Wang, H., Legg, S., & Hallberg, R. W. (2015). Representations of the Nordic Seas overflows and their large scale climate impact in coupled models. *Ocean Modelling*, *86*, 76–92. https://doi.org/10.1016/j.ocemod.2014.12.005
Wang, Q., Danilov, S., Sidorenko, D., Timmermann, R., Wekerle, C., Wang, X., et al. (2014). The Finite Element Sea Ice-Ocean Model (FESOM) v. 1.4: Formulation of an ocean general circulation model. *Geoscientific Model Development*, *7*(2), 663–693. https://doi.org/10.5194/gmd-7-663-2014
Webb, D. J., Coward, A. C., de Cuevas, B. A., & Gwillam, C. S. (1997). A multiprocessor ocean general circulation model using message passing. *Journal of Atmospheric and Oceanic Technology*, *14*, 175–183.
Webb, D.J., , B. A. de Cuevas, and A. C. Coward, 1998: The first main run of the OCCAM global ocean model. James Rennell Division Internal Rep. 34, Southampton Oceanography Centre, 50 pp. [Avail- able online at http://www.soc.soton.ac.uk/JRD/OCCAM.]
Weber, S. L., & Drijfhout, S. S. (2007). Stability of the Atlantic meridional overturning circulation in the last glacial maximum climate. *Geophysical Research Letters*, *34*, L22706. https://doi.org/10.1029/2007GL031437
Weijer, W., Cheng, W., Drijfhout, S. S., Fedorov, A. V., Hu, A., Jackson, L. C., et al. (2019). Stability of the Atlantic Meridional Overturning Circulation: A Review and Synthesis. *Journal of Geophysical Research: Oceans*, *124*, 5336–5375. https://doi.org/10.1029/2019JC015083
Weijer, W., de Ruijter, W. P., Dijkstra, H. A., & Van Leeuwen, P. J. (1999). Impact of interbasin exchange on the Atlantic overturning circulation. *Journal of Physical Oceanography*, *29*(9), 2266–2284.
Weijer, W., Maltrud, M., Hecht, M., Dijkstra, H., & Kliphuis, M. (2012). Response of the Atlantic Ocean circulation to Greenland Ice Sheet melting in a strongly-eddying ocean model. *Geophysical Research Letters*, *39*, L09606. https://doi.org/10.1029/2012GL051611
Weijer, W., & Van Sebille, E. (2014). Impact of Agulhas leakage on the Atlantic overturning circulation in the CCSM4. *Journal of Climate*, *27*(1), 101–110.
Willis, J. K. (2010). Can in situ floats and satellite altimeters detect long-term changes in Atlantic Ocean overturning? *Geophysical Research Letters*, *37*, L06602. https://doi.org/10.1029/2010GL042372
Williamson, D., Blaker, A., & Sinha, B. (2017). Tuning without over-tuning: parametric uncertainty quantification for the NEMO ocean model. *Geoscientific Model Development*, *10*, 1789–1816. https://doi.org/10.5194/gmd-10-1789-2017
Williamson, D., Goldstein, M., Allison, L., Blaker, A., Challenor, P., Jackson, L., & Yamazaki, K. (2013). History matching for exploring and reducing climate model parameter space using observations and a large perturbed physics ensemble. *Climate Dynamics*, *41*(7-8), 1703–1729. https://doi.org/10.1007/s00382-013-1896-4
Winton, M., Anderson, W. G., Delworth, T. L., Griffies, S. M., Hurlin, W. J., & Rosati, A. (2014). Has coarse ocean resolution biased simulations of transient climate sensitivity? *Geophysical Research Letters*, *41*, 8522–8529. https://doi.org/10.1002/2014GL061523
Winton, M., Hallberg, R. W., & Gnanadesikan, A. (1998). Simulation of density-driven frictional downslope flow in z-coordinate ocean models. *Journal of Physical Oceanography*, *28*, 2163–2174.
Wolfe, C. L., & Cessi, P. (2014). Salt feedback in the adiabatic overturning circulation. *Journal of Physical Oceanography*, *44*(4), 1175–1194.
Wolfe, C. L., & Cessi, P. (2015). Multiple regimes and low-frequency variability in the quasi-adiabatic overturning circulation. *Journal of Physical Oceanography*, *45*(6), 1690–1708.
Wood, R. A., Rodríguez, J. M., Smith, R. S., Jackson, L. C., & Hawkins, E. (2019). Observable, low-order dynamical controls on thresholds of the Atlantic Meridional Overturning Circulation. *Climate Dynamics*, *53*(11), 6815–6834.
Wunsch, C. (2008). Mass and volume transport variability in an eddy-filled ocean. *Nature Geoscience*, **1**(3), 165-168. Wunsch, C., & Ferrari, R. (2004). Vertical mixing, energy, and the general circulation of the oceans. *Annual Review of Fluid Mechanics*, *36*, 281–314.
Wunsch, C., & Heimbach, P. (2006). Estimated decadal changes in the North Atlantic meridional overturning circulation and heat flux 1993–2004. *Journal of Physical Oceanography*, *36*(11), 2012–2024.
Xu, X., Bower, A., Furey, H., & Chassignet, E. P. (2018). Variability of the Iceland-Scotland overflow water transport through the Charlie-Gibbs Fracture Zone: Results from an eddying simulation and observations. *Journal of Geophysical Research: Oceans*, *123*, 5808–5823. https://doi.org/10.1029/2018JC013895
Xu, X., Chassignet, E. P., Johns, W. E., Schmitz, W. J., & Metzger, E. J. (2014). Intraseasonal to interannual variability of the Atlantic meridional overturning circulation from eddy-resolving simulations and observations. *Journal of Geophysical Research: Oceans*, *119*, 5140–5159. https://doi.org/10.1002/2014JC009994
Xu, X., Hurlburt, H. E., Schmitz, W. J., Zantopp, R., Fischer, J., & Hogan, P. J. (2013). On the currents and transports connected with the Atlantic meridional overturning circulation in the subpolar North Atlantic. *Journal of Geophysical Research: Oceans*, *118*, 502–516. https://doi.org/10.1002/jgrc.20065
Xu, X., Rhines, P. B., Chassignet, E. P., & Schmitz, W. J. Jr. (2015). Spreading of the Denmark Strait overflow water in the western subpolar North Atlantic: Insights from eddy-resolving simulations with a passive tracer. *Journal of Physical Oceanography*, *45*(12), 2913–2932. https://doi.org/10.1175/JPO-D-14-0179.1
Xu, X., Schmitz, W. J., Hurlburt, H. E., & Hogan, P. J. (2012). Mean Atlantic meridional overturning circulation across 26.5°N from eddy-resolving simulations compared to observations. *Journal of Geophysical Research*, *117*, C03042. https://doi.org/10.1029/2011JC007586
Xu, X., Schmitz, W. J. Jr., Hurlburt, H. E., Hogan, P. J., & Chassignet, E. P. (2010). Transport of Nordic Seas overflow water into and within the Irminger Sea: An eddy-resolving simulation and observations. *Journal of Geophysical Research*, *115*, C12048. https://doi.org/10.1029/2010JC006351
Yeager, S., Karspeck, A., & Danabasoglu, G. (2015). Predicted slowdown in the rate of Atlantic sea ice loss. *Geophysical Research Letters*, *42*, 10,704–10,713. https://doi.org/10.1002/2015GL065364 Zhang, R. (2010). Latitudinal dependence of Atlantic Meridional Overturning Circulation (AMOC) variations. *Geophysical Research Letters*, *37*, L16703. https://doi.org/10.1029/2010GL044474
Zhang, R., Sutton, R., Danabasoglu, G., Kwon, Y. O., Marsh, R., Yeager, S. G., et al. (2019). A review of the role of the Atlantic Meridional Overturning Circulation in Atlantic multidecadal variability and associated climate impacts. *Reviews of Geophysics*, *57*, 316–375. https://doi.org/10.1029/2019RG000644
Zika, J. D., England, M. H., & Sijp, W. P. (2012). The ocean circulationin thermohaline coordinates. *Journal of Physical Oceanography*, *2*, 708–724.